AD-A096 279 NAVAL RESEARCH LAB WASHINGTON DC F/G 4/1
PLUMEX II. A SECOND SET OF COINCIDENT RADAR AND ROCKET OBSERVAT--ETC(U)
DEC 80 E P SZUSZCZEWICZ, R T TSUNODA
UNCLASSIFIED NRL-MR-4344 NL

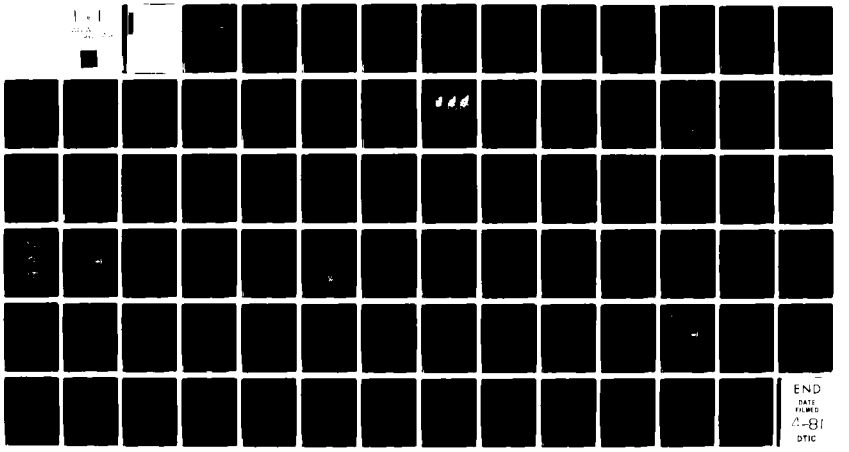

END
DATE FILMED
4-81
DTIC

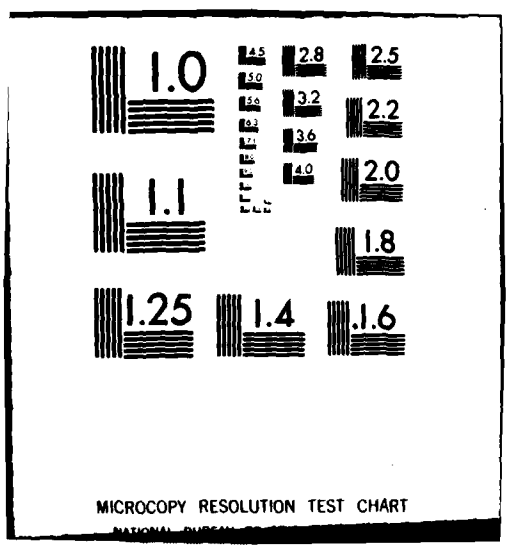
1.0
1.1
1.25
1.4
1.6
1.8
2.0
2.2
2.5
2.8
3.2
3.6
4.0
4.5
5.0
5.6
6.3
7.1
MICROCOPY RESOLUTION TEST CHART

SECURITY CLASSIFICATION OF THIS PAGE (When Data Entered)

REPORT DOCUMENTATION PAGE

READ INSTRUCTIONS BEFORE COMPLETING FORM

1. REPORT NUMBER: NRL Memorandum Report 4344
2. GOVT ACCESSION NO.: AD-A096279
3. RECIPIENT'S CATALOG NUMBER:

4. TITLE (and Subtitle): PLUMEX II: A SECOND SET OF COINCIDENT RADAR AND ROCKET OBSERVATIONS OF EQUATORIAL SPREAD-F
5. TYPE OF REPORT & PERIOD COVERED: Interim report on a continuing NRL problem.
6. PERFORMING ORG. REPORT NUMBER: NRL-MR-4344

7. AUTHOR(s): E.P. Szuszczewicz, R.T. Tsunoda, R. Narcisi, J.C. Holmes
8. CONTRACT OR GRANT NUMBER(s):

9. PERFORMING ORGANIZATION NAME AND ADDRESS: Naval Research Laboratory, Washington, D.C. 20375
10. PROGRAM ELEMENT, PROJECT, TASK AREA & WORK UNIT NUMBERS: 61153N; RR033-02-44; 71-0949-0-0, and 71-0950-0-0

11. CONTROLLING OFFICE NAME AND ADDRESS: Office of Naval Research, Arlington, VA 22217
12. REPORT DATE: December 30, 1980
13. NUMBER OF PAGES: 82

14. MONITORING AGENCY NAME & ADDRESS (if different from Controlling Office): RR033-02, I25AAXH; RR033-02-44, X640
15. SECURITY CLASS. (of this report): UNCLASSIFIED
15a. DECLASSIFICATION/DOWNGRADING SCHEDULE:

16. DISTRIBUTION STATEMENT (of this Report)

Approved for public release; distribution unlimited.

17. DISTRIBUTION STATEMENT (of the abstract entered in Block 20, if different from Report)

18. SUPPLEMENTARY NOTES

*Address: SRI International, 333 Ravenwood Avenue, Menlo Park, California 94025.
†Address: Air Force Geophysics Laboratory, Hanscom Air Force Base, Massachusetts 01731.
This work was partially funded by the Defense Nuclear Agency under subtask I25AAXHX640, work unit 12, and work unit title "Nuclear Weapons and Ionospheric Effects."

19. KEY WORDS (Continue on reverse side if necessary and identify by block number)

Measurements of equatorial spread-F
Irregularities
Backscatter plumes

20. ABSTRACT (Continue on reverse side if necessary and identify by block number)

PLUMEX II was the second in a two-rocket operation that successfully executed space- and time-coincident measurements of equatorial spread-F. The first launch operation (PLUMEX I) was conducted during the late phase in the development and decay of spread-F; major radar plume features were relatively stable with respect to vertical drifts, and the most intense regions of radar backscatter were beginning to decay. The PLUMEX II conditions were substantially different, with the rocket having been launched into the mid-phase of well-developed spread-F, i.e., a ground-based ionosonde showed full range spread while Altair radar maps of meter-size irregularities displayed backscatter plumes that penetrated to the topside F-layer and continued rising with time. Current analysis of

(Continues)

DD FORM 1 JAN 73 1473 EDITION OF 1 NOV 65 IS OBSOLETE
S/N 0102-LF-014-6601

SECURITY CLASSIFICATION OF THIS PAGE (When Data Entered)

251950

AD-A096279

To: Distribution list for NRL Memorandum Report 4344, "PLUMEX II: A Second Set of Coincident Radar and Rocket Observations of Equatorial Spread-F," by E.P. Szuszczewicz, J.C. Holmes, R.T. Tsunoda, and R. Narcisi, dated December 30, 1980.

The following was inadvertently omitted from page ii:

20. Abstract (Continued)

PLUMEX II results show that F-region irregularities were observed only on the bottomside gradient with $F_2{}^h{}_{max}$ at 510 km and $N_e^{max} \approx 6(10^5)$ cm^{-3}. Smaller scale irregularities (i.e., small scale structure imbedded in larger scale features) appear less intense than corresponding observations in PLUMEX I. If substantiated by more quantitative analyses, this result could support current interpretations of east-west plume asymmetry which suggests that the western wall of a plume (the PLUMEX I case) is more unstable than its eastern counterpart (the PLUMEX II case). With regard to ion composition, NO^+ was the dominant positive-charge component at altitudes below the F-region ledge. Across the ledge and throughout the F-layer up to an apogee of 580 km O^+ dominated. The ion results support a model of a Rayleigh-Taylor mode which assumes relatively small depletions originating on the F-ledge with initially small horizontal extent. In this model, the local ion composition will be transported to higher altitudes but molecular ions will not be the dominant positive species.

CONTENTS

PLUMEX II: A SECOND SET OF COINCIDENT RADAR AND ROCKET OBSERVATIONS OF EQUATORIAL SPREAD-F

I. INTRODUCTION

The coordinated measurements of equatorial spread-F conducted during July 1979 at the Kwajalein Atoll involved the launch of two instrumented rocket payloads designed to probe the detailed "in situ" structure of the turbulent ionospheric plasma. The first launch operation (PLUMEX I; 17 July 1979; 0031:30.25 LT) was conducted during the late phase in the development and decay of spread-F. The associated results and discussions of ground-based and rocket-borne diagnostics have been presented in companion papers[1,2]. The second rocket (PLUMEX II: 23 July 1979; 2157:30 LT) was launched into the mid-phase of well-developed spread-F, i.e., a ground-based ionosonde showed full frequency and range spread while the Altair radar maps of meter size irregularity contours displayed backscatter plumes that penetrated to the topside F-layer and continued rising with time. We present here the initial PLUMEX II observations of radar plumes and the "in situ" measurements of the rocket-borne plasma probes and mass spectrometer. The results are then compared with PLUMEX I.

Manuscript submitted July 25, 1980.

II. EXPERIMENTAL RESULTS

A. Ionospheric Conditions and Radar Maps

By 2000 hr LT on the night of the PLUMEX II launch, ionograms showed that the virtual height (h'F) of the F-layer had risen at an average rate of 12 meters/sec to an altitude of 350 km. At that point vertical drifting ceased and shortly thereafter full-range spread-F was observed. The virtual height remained constant until 2130 hr LT, when upward drifting again commenced at an average rate of 18 meters/sec. With full-range spread-F still in effect and with the F-layer still drifting at an upward rate near 18 meters/sec the PLUMEX II rocket was launched (0957:30 UT on day 205; 2157:30, 23 July 1979, LT).

Operating at 155.5 MHz (radar backscatter from 1 m field-aligned irregularities) the Altair radar executed consecutive magnetic east-west scans in a plane that included the upleg penetration of the rocket trajectory. Figure 1 presents the contours of constant backscatter strength[3] plotted in increments of 10 dB, ranging from 0 dB (domain of small dots) to 50 dB (solid black). The first panel in Figure 1 shows backscatter returns extending from 350 to 1000 km, with the most intense region (50 dB level) centered at 635 km. A measure of horizontal and vertical drift velocity can be achieved by focussing on features "α" (the 50 dB region at 635 km) and "β" (the 20 dB region at an

altitude of 550 km, and 125 km west of Altair in the first panel). In the 135 sec time lapse between the radar measurements in panels 1 and 2, the observations showed that (V_α (hor), V_α (vert)) $\approx$ (290 m/sec, 170 m/sec) and (V_β (hor), V_β (vert)) $\approx$ (300 m/sec, 150 m/sec). The results can be interpreted as an average magnetic west-to-east plume drift velocity of 295 m/sec (about 130 m/sec faster than corresponding observations in PLUMEX I) with a corresponding average upward vertical drift velocity equal to 160 m/sec. (Note that ionograms showed h'F moving upward at an average rate of 18 m/sec throughout most of the time encompassed by the radar maps in Figure 1. Therefore, one could conclude that the plume was drifting upward at a rate of 142 m/sec relative to the F-layer bottomside.) In the 124 second interval between panels 2 and 3 the average magnetic west-to-east drift velocity was considerably lower, with a rate at 100 m/sec. During this same interval the average vertical drift velocity increased to 270 m/sec (252 m/sec relative to the bottomside F-region).

B. Rocket Profile and Comparison with Radar

The rocket payload that was launched into the spread-F conditions depicted in Figure 1 carried, among other instruments, a quadrupole ion mass spectrometer and a pair of pulsed plasma probes (See Ref. 2 for instrument details and the payload configuration). The pair of pulsed probes simultaneously tracked ion and electron saturation currents while generating conventional Langmuir probe characteristics[2]. Figure 2 displays the upleg measurements

of relative electron density as observed by electron saturation currents I_B^e and corroborated by simultaneously measured ion saturation currents. Because ion and electron saturation currents have significantly different sensitivities to velocity, sheath and magnetic field effects, variations in one polarity current not corroborated by the other were attributed to the various aspect sensitivities and excluded from Figure 2. This approach not only facilitates quick-look analysis and established credibility in the interpretation of the curves as relative electron density profiles, but also proved to be a valuable technique for eliminating the otherwise degrading effects of uncontrolled payload tumple and ACS jet firings that resulted from the failure of payload separation from the rocket motor in PLUMEX II. The ordinate in Figure 2 has a linear scale for time-after-launch with altitude superimposed at 50 second increments.

The profile shows that the payload entered the very bottom of the F-layer at $t \tilde{-} 145$ sec ($Z \tilde{\approx} 340$ km), a point designated "A" in Figure 2. From there to an apogee near 581 km (t = 390 sec) the "in situ" probe measurements revealed a number of irregular structures, all contiguous and co-located on the bottomside gradient between points "B" and "C" in Figure 2. From the F-peak to the topside apogee of 581 km there were no "in situ" observations of macroscale depletions or smaller scale irregularities as reported in PLUMEX I (Ref. 1).

The payload's upleg trajectory has been superimposed on the radar maps in Figure 1. With regions A through E (and

their associated times of observation) identified on the panel best matched for time coincidence. A step-wise comparison of "in situ" observations (Fig. 2) with the radar maps shows the following correlations:

Point "A" in Figures 1 and 2 corresponds to the lowest position of the bottomside F-layer, a result which co-locates the very bottom of the F-region radar returns with the very bottom of the F-region ledge. Before PLUMEX I and II (an identical correlation was found in PLUMEX I) there were no data to determine their co-location or lack thereof.

The transition from locations A to B is marked by a 20 dB increase in radar backscatter energy, while region B to C is marked by a relatively constant domain of backscatter energy.

Observations at D and E occur along the eastern "wall" of the plume and encompass an altitude domain stretching from the F-layer peak near 500 km to a topside altitude near the vehicle apogee of 580 km.

Figure 3 presents the up- and downleg profiles of relative electron density as measured by "in situ" probe baseline electron saturation currents. (The integrity of the downleg profile was established by the same procedure utilized in Figure 2.) A comparison of the profiles shows the downleg results more representative of an undisturbed F-region, a result consistent with the rocket's west-to-east movement relative to the radar plume. This relative motion (approximately 160 m/sec) carried the rocket payload into the undisturbed F-region just to the east of the observed

radar plume (i.e., into the white region on the eastern edge of the first panel in Figure 1).

A comment is in order with regard to the up- and downleg altitudes that have been superimposed at 50 second intervals in Figure 3. In particular, attention is directed to the locations of the very bottom of the two F-region ledge observations, 340 km upleg and 305 km downleg. Because of the 9^{o} dip in the local geomagnetic field the downleg observation at 650 sec corresponds to 338 km when projected along the magnetic field line to the payload position at 145 sec upleg, a result showing virtually no net movement of the ledge between the up and downleg observations. (We note that at the time of launch ionograms showed h'F rising at an approximate rate of 18 m/sec. This vertical drift then reversed near the middle of the flight, establishing consistency in rocket and ionogram results.)

With regard to ion composition, we note that the molecular ion NO^{+} was the dominant positive-charge component at altitudes up to 340 km, the very bottom of the F-region ledge ("A" in Figure 2). At all altitudes above 340 km O^{+} was observed to be the dominant ion (See Ref. 4 for detailed ion profiles).

III. CONCLUSIONS AND COMPARISONS WITH PLUMEX I

PLUMEX II was the second in a two-rocket operation that successfully executed space- and time-coincident measurements of equatorial spread-F. Comparison of results and

focus on differences in prevailing ionospheric conditions can be achieved by an analysis of the upleg electron density profiles observed in the two operations (PLUMEX I and II). These profiles are presented in Figure 4 with specific features and conditions of observation listed in Table 1.

TABLE 1

A COMPARISON OF CONDITIONS AND OBSERVATIONS IN THE DNA/PLUMEX CAMPAIGN

	PLUMEX I	PLUMEX II
Launch Time (LT)	17 July 1979; 0031:30.25	23 July 1979; 2157:30
Spread-*F* Conditions	Late time; topside radar plume in decay phase	Mid-phase of well-developed spread-*F*; plumes penetrating to topside and rising with time
$F_2 h_{max}$	375 Km	510 Km
F-bottom	240 Km	340 Km
N_e^{max}	1.3 (10^6) cm^{-3}	$\approx$ 6(10^5) cm^{-3}
L (Gradient scale length)	4.0 Km	8.6 Km
T_e	1350 ($\pm$250)°K	TBD
Dominant F_2 Ion	0^+	0^+
Number of Depletions ($\Delta N_e/N_e^0 \geq .60$)	4	Only Bottomside Spread-*F*
Maximum Depletion $(\Delta N_e/N_e^0)_{max}$	0.90	$\approx$ 0.75 (An estimate of bottomside macroscale structure)
"In Situ" Irregularity Strength	$\pm$80% fluctuations on bottomside gradient	Fluctuation levels are much less intense than PLUMEX I
Ion Signatures in Holes	$N^+/0^+$ ratio	None
Plume Penetration by Rocket	Western "wall" and plume "head"	Eastern "wall"

Spread-F conditions. PLUMEX I was conducted during the late phase in the development and decay of spread-F. Specifically, the rocket was launched at 0031:30.25 (LT), a full 3 hrs after the occurrence of full range spread and only 30 minutes before its disappearance from ground-based ionograms. Major plume features were relatively stable with respect to vertical drifts, and the most intense regions of radar backscatter were beginning to decay.

The PLUMEX II conditions were substantially different, with the rocket having been launched into the mid-phase of well-developed spread-F, i.e., a ground-based ionosonde showed full-frequency and range spread while the Altair radar maps of meter size irregularity contours displayed backscatter plumes that penetrated to the topside F-layer and continued rising with time. The payload was launched 1½ hours after the onset of full range spread and an estimated two hours before decay.

F-region profiles and "in situ" irregularities. In the PLUMEX I operation, a number of major depletions ($\Delta N_e/N_e^o \lesssim 0.90$) were distributed throughout the F-region with the F-peak (F_2h_{max}) at 375 Km and $N_e^{max} = 1.3\ (10^6)\ cm^{-3}$ ($\pm$ 10%). The very bottom of the F-layer (F-bottom) was at 240 km and the macroscopic gradient scale length $L^{-1} = (N_e^o)^{-1}\ dN_e^o/dz$ of the bottomside ledge was 4.0 Km. (The macroscopic L was calculated from a zero-order fit to the bottomside ledge between 10^{-2} and $10^{-1}\ N_e^{max}$.) The electron energy distribution was characterized by $T_e = 1350\ (\pm 250)^oK$ with no obvious

signatures of energy redistribution in and around the depletions. The most intense "in situ" irregularities (i.e., smaller scale structure imbedded in the larger scale depletions) occurred near 275 km on the bottomside ledge ($\pm$ 80% fluctuations about an estimate N_e^o). The power spectral density in this region of intense irregularities on the bottomside was dominated by a $k^{-2.5}$ power law[2] over the intermediate wavelength domain $k = 2\pi/1$ km to $k = 2\pi/25$ m. This result supports the role of the collisional Rayleigh-Taylor instability in generating intermediate wavelength irregularities[2,5,6] during the occurrence of equatorial spread-F (See References 1 and 2 for additional details.)

The PLUMEX II data have not received the same level of analysis already applied to the first operation, a result largely due to the complications of uncontrolled payload tumble and ACS jet firings that arose from a subsystem failure to separate the science payload from the second stage rocket motor. However, there are a number of conclusions that can be drawn at this time. In the upleg density profile of the PLUMEX II flight (Fig. 2), F-region irregularities were observed only on the bottomside gradient, with the F-peak (F_2h_{max}) at 510 km and $N_e^{max} \approx 6(10^5)$ cm^{-3}. In PLUMEX II the bottomside gradient was substantially softer than in PLUMEX I with F-bottom at 340 km and L = 8.6 km. A review of analog records (uncorrected for tumble and jet firings) indicates that smaller scale "in situ" irregularities were much less intense than corresponding observations in PLUMEX I. This

result could support current interpretations (e.g., Ref. 7) of east-west plume asymmetry which suggest that the western wall of a plume (the PLUMES I case) is more unstable than its eastern counterpart (the PLUMEX II case).

Ion composition. PLUMEX I and II provided the very first vertical profiles of ion composition during the occurrence of equatorial spread-F. The data are particularly relevant to the subject of plasma bubble formation, vertical transport and ion signatures of source domains for topside F-region depletions. Previous "in situ" measurements of ion composition within plasma depletions came only from satellite-borne mass spectrometers[8-10] with results that suggested that topside holes formed at lower altitudes, where $[NO^+]$, $[O_2^+] > [O^+]$, and rise to greater heights maintaining (to first-order) their original ion composition. In a final analysis, the composition can be different because of dependence on the bubble formation process, the source domain and the bubble age as manifested by time-dependent chemical processes.

In both PLUMEX operations O^+ was the dominant F-region ion down to the very bottom of the F-ledge (F-bottom). At altitudes below F-bottom, molecular ions dominated with a scale height approaching infinity. (Detailed ion chemical results and analyses that go beyond discussions presented here are available in Reference 4.) The connection of this observation to topside bubbles and instability mechanisms is as follows:

The Rayleigh-Taylor and $\bar{E} \times \bar{B}$ gradient drift instabilities, which have been proposed for bubble formation, require a steep bottomside gradient. However, the PLUMEX results show that the molecular ions are dominant only at altitudes below the bottomside F-region gradient, where scale heights are very large and inhibit the instability process. If the bubble does indeed form on the F-region ledge, and if it transports only local ions to higher altitudes, then molecular ions will never dominate topside depletions. This apparent dichotomy has a number of explanations:

(a) Relatively small depletions (i.e., $\Delta N_e/N_e^o \lesssim 0.9$) originating on the F-ledge with initially small horizontal extent can transport the local ion composition to higher altitudes by the Rayleigh-Taylor process; but molecular ions will not be the dominant positive species. Instead, the $[N^+]/[O^+]$ ratio will indicate the original source domain as suggested by McClure et al.[8] and Szuszczewicz et al.[1], and discussed in detail by Narcisi and Szuszczewicz[4].

(b) For molecular ions to be dominant in a topside F-region depletion it appears that one of two mechanisms must apply: (i) An initially small depletion (i.e., $\Delta N_e/N_e^o \lesssim 0.9$) of large horizontal scale size can result in much higher depletion levels (e.g., References 8-10) by fringing fields that drawup the lower densities and molecular ions that populate altitude regimes lower than the sight of the initial perturbation. This mechanism has been studied by Zalesak and Ossakow[11] and appears in substantial agreement with observations.

(c) An alternate mechanism for molecular ion dominance in topside depletions has been proposed by Chiu and Straus[12]. They suggest that plasma bubbles in the nighttime equatorial ionosphere originate as wind driven waves at one of the highly variable density gradients below 200 km, rather than at the bottomside F-region ledge. Once the bubble is formed, with the low densities and molecular ion dominance characterized by the lower altitude, it can propogate into the bottomside F-region and provide the initial perturbation required for the onset of the Rayleigh-Taylor mode[13-15].

Current analyses of PLUMEX ion composition results support conclusion "a" as the operating principle on the nights of "in situ" investigations. This does not negate "b" and "c" as candidates for other conditions, but it does leave open the question for further experimental tests.

ACKNOWLEDGMENTS

Support for the plasma probe analysis was provided by the Defense Nuclear Agency (DNA) under Subtask Code I25AAXHX640, Communications Effects Experiments. The Altair radar analysis was also supported by DNA under contract DNA 001-C-0153. Support for the ion composition measurements was supplied mostly by the Air Force Office of Scientific Research under Task 2310-G3 and partially by DNA under Subtask I25AAXHX640, Work Unit 06. We also wish to acknowledge the dedicated technical support of E. Trzcinski, G. Federico, L. Wlodyka, L. Kegley, D. Walker and C. S. Lin, who independently and as a

team contributed significantly to the success of the rocket-borne plasma probe and mass spectrometer experiments. Development of the plasma probe technique was provided by the Office of Naval Research under Work Unit A02-11.11 (71-0949-0-0), Ionospheric and Stratospheric Interactions, Task Area RR 043-02-044.

REFERENCES

1. Szuszczewicz, E.P., R.T. Tsunoda, R. Narcisi and J.C. Holmes, "PLUMEX I: Coincident radar and rocket observations of equatorial spread-F," Appendix A, also published in Geophys. Res. Lett. 7, 537 (1980).
2. Szuszczewicz, E.P. and J.C. Holmes, "The pulsed-plasma-probe experiment: "In situ" measurements of electron density, temperature and density fluctuation power spectra," Appendix B, also published in NRL Memorandum Rpt. 4289 (July 1980).
3. Tsunoda, R.T., M.J. Baron, J. Owen and D.M. Towle, "Altair: An incoherent scatter radar for equatorial spread-F studies," Radio Sci. 14, 1111 (1979).
4. Narcisi, R., and E.P. Szuszczewicz, "Direct measurements of electron density, temperature and ion composition in an equatorial spread-F ionosphere", presented as paper 3-16 Sixth International Symposium on Equatorial Aeronomy, Puerto Rico (July 1980); to be published in J. Atm. Terr. Phys., (1981, special issue).

5. Keskinen, M.J., S.L. Ossakow and P.K. Chaturvedi, "Preliminary report on numerical simulations of intermediate wavelength collisional Rayleigh-Taylor instability in equatorial spread-F," J. Geophys. Res. 85, 1775 (1980).

6. Keskinen, M.J., E.P. Szuszczewicz, S.L. Ossakow and J.C. Holmes, "Nonlinear theory and experimental observations of the local collissional Rayleigh-Taylor instability in a descending equatorial spread-F ionosphere," J. Geophys. Res. (Oct. 1980 submitted).

7. Tsunoda, R.T., "Time evolution and dynamics of equatorial backscatter plumes - Growth phase," SRI International Rpt (in press, 1980).

8. McClure, J.P., W.B. Hanson and J.H. Hoffman, "Plasma bubbles and irregularities in the equatorial ionosphere," J. Geophys. Res. 82, 2650 (1977).

9. Brinton, H.C., H.G. Mayr, and G.F. Newton, "Ion composition in the nighttime equatorial F-region: Implications for chemistry and dynamics", (abstract), EOS Trans. AGU, 56, 1038, (1975).

10. Szuszczewicz, E.P., "Ionospheric holes and equatorial spread-F: Chemistry and transport," J. Geophys. Res. 83, 2665, (1978).

11. Zalesak, S.T., and S.L. Ossakow, "Nonlinear equatorial spread F: Spatially large bubbles resulting from large horizontal scale initial perturbations," NRL Memorandum Rpt 4154 (February 6, 1980); J. Geophys. Res. 85, 2131, (1980).

12. Chiu, Y.T. and J.M. Straus, "Rayleigh-Taylor and wind-driven instabilities of the nighttime equatorial ionosphere," J. Geophys. Res. 84, 3283 (1979).

13. Scannapieco, A.J., and S.L. Ossakow, "Nonlinear equatorial spread-F," Geophys. Res. Lett. 3, 451 (1976).

14. Ott, E., "Theory of Rayleigh-Taylor bubbles in the equatorial ionosphere," J. Geophys. Res. 83, 2066 (1978).

15. Chaturvedi, P.K., and S.L. Ossakow, "Nonlinear theory of the collisional Rayleigh-Taylor instability in equatorial spread-F," Geophys. Res. Lett. 4, 558 (1977).

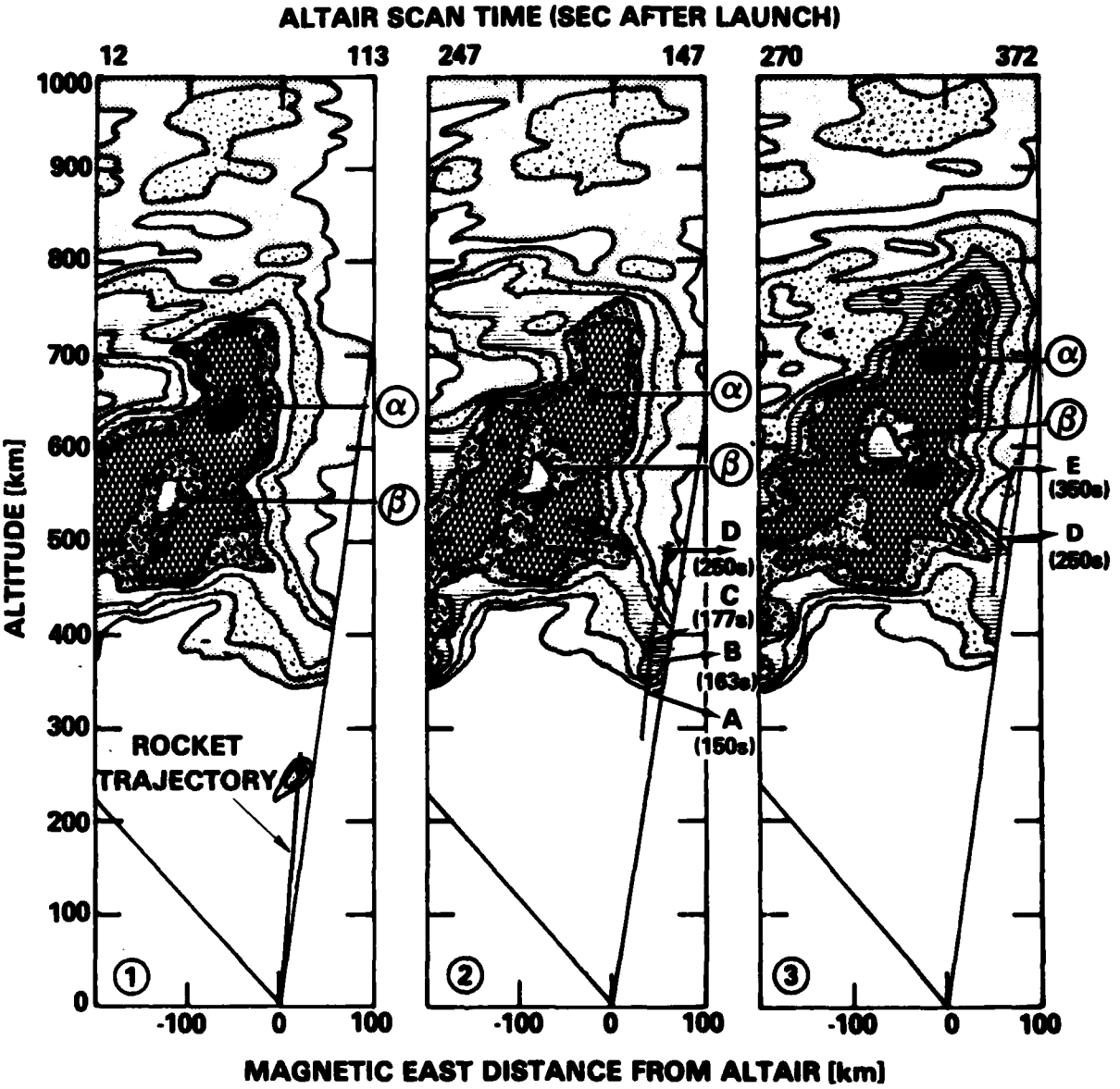

Fig. 1 - Backscatter intensity contour maps (contours are in 10 dB increments with darkest domain, e.g., α , at the 50 dB level) with superposition of the rocket trajectory. The times identified with observations "A" through "F" are included for a more complete representation of temporal correlation with the successive radar scans. Domains "α" and "β" are references for plume dynamics (see text).

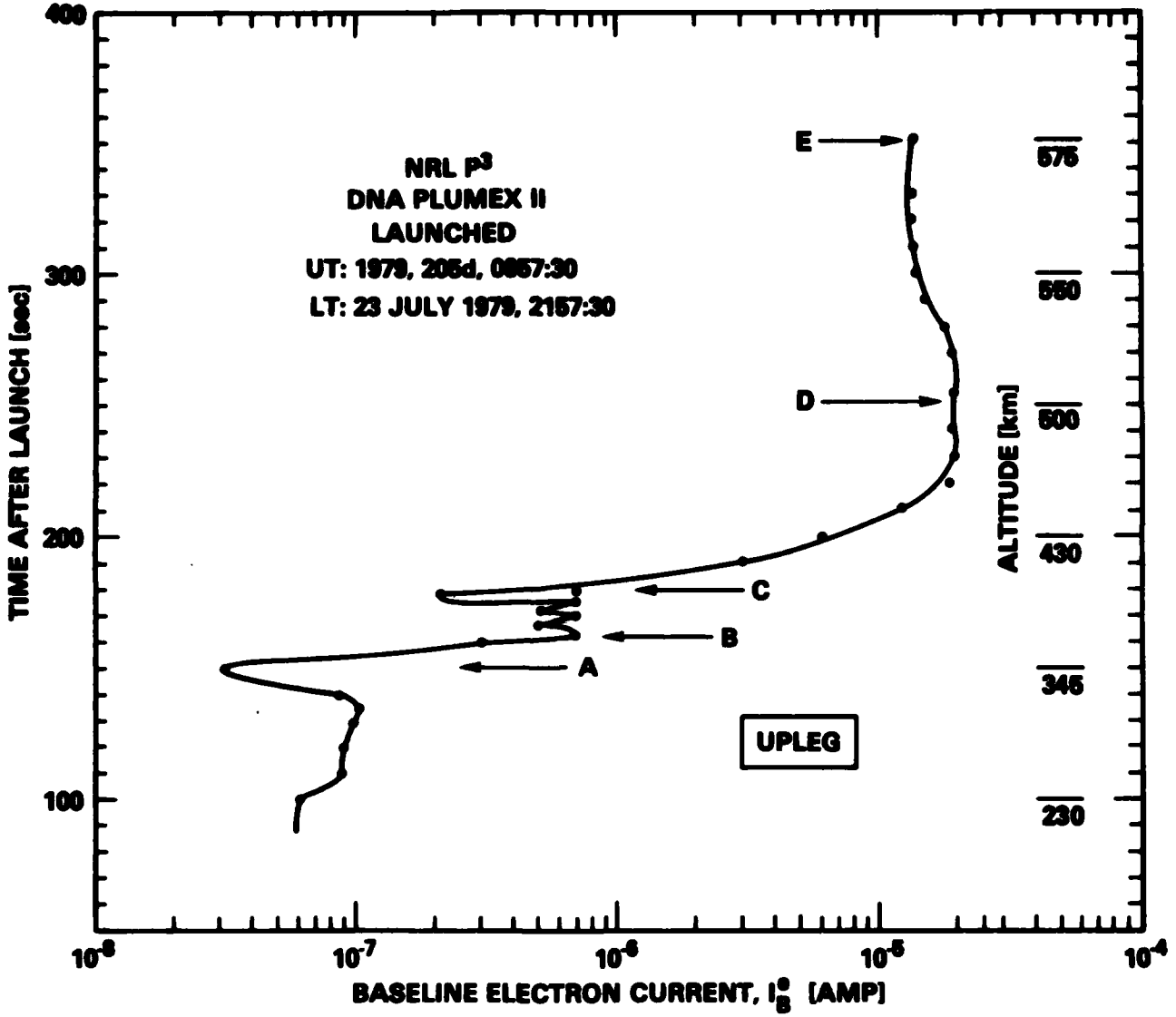

Fig. 2 - Relative electron density profile as measures simultaneously by ion and electron saturation probe currents collected on the upleg trajectory.

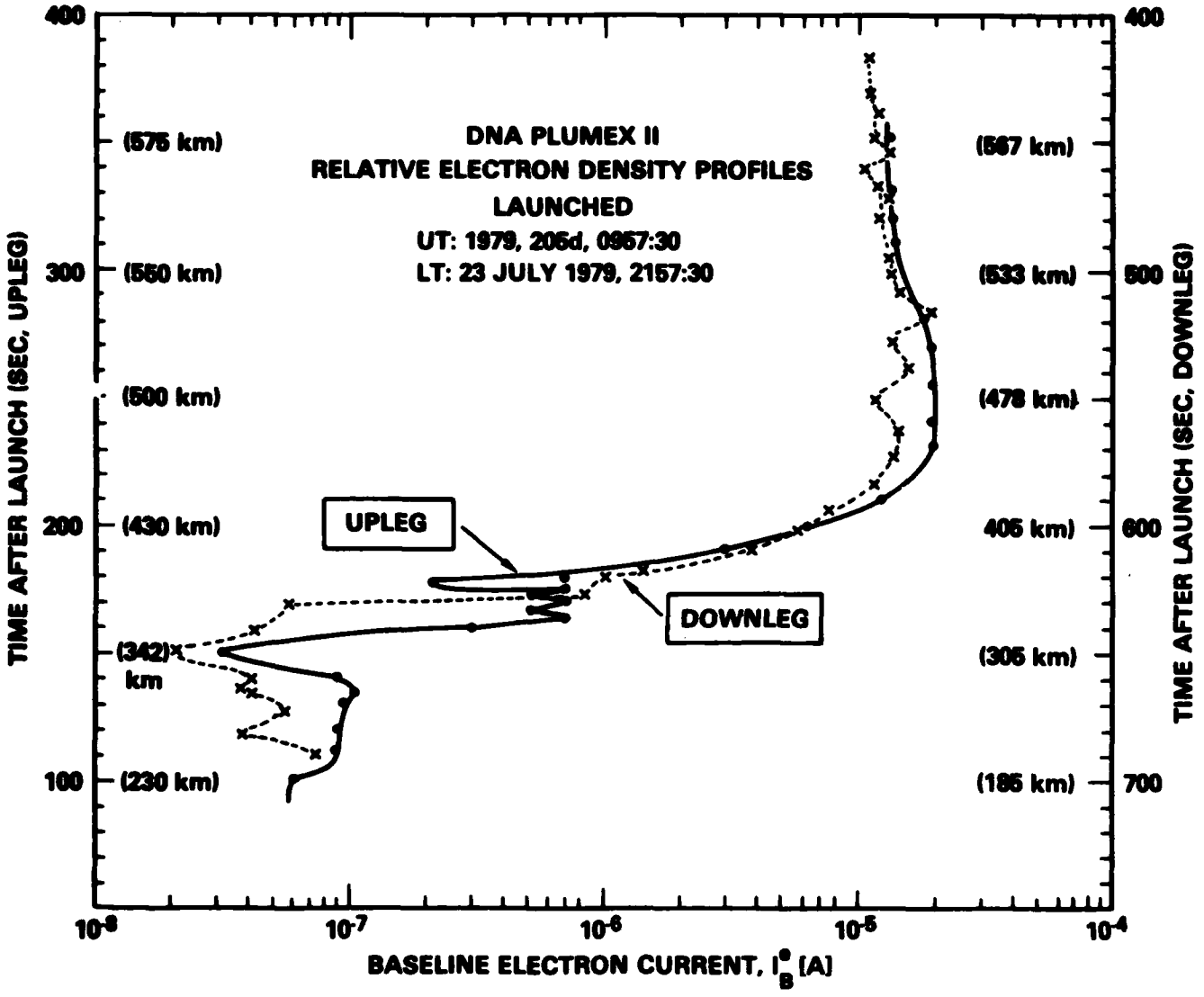

Fig. 3 - Comparison of up- and downleg plasma profiles.

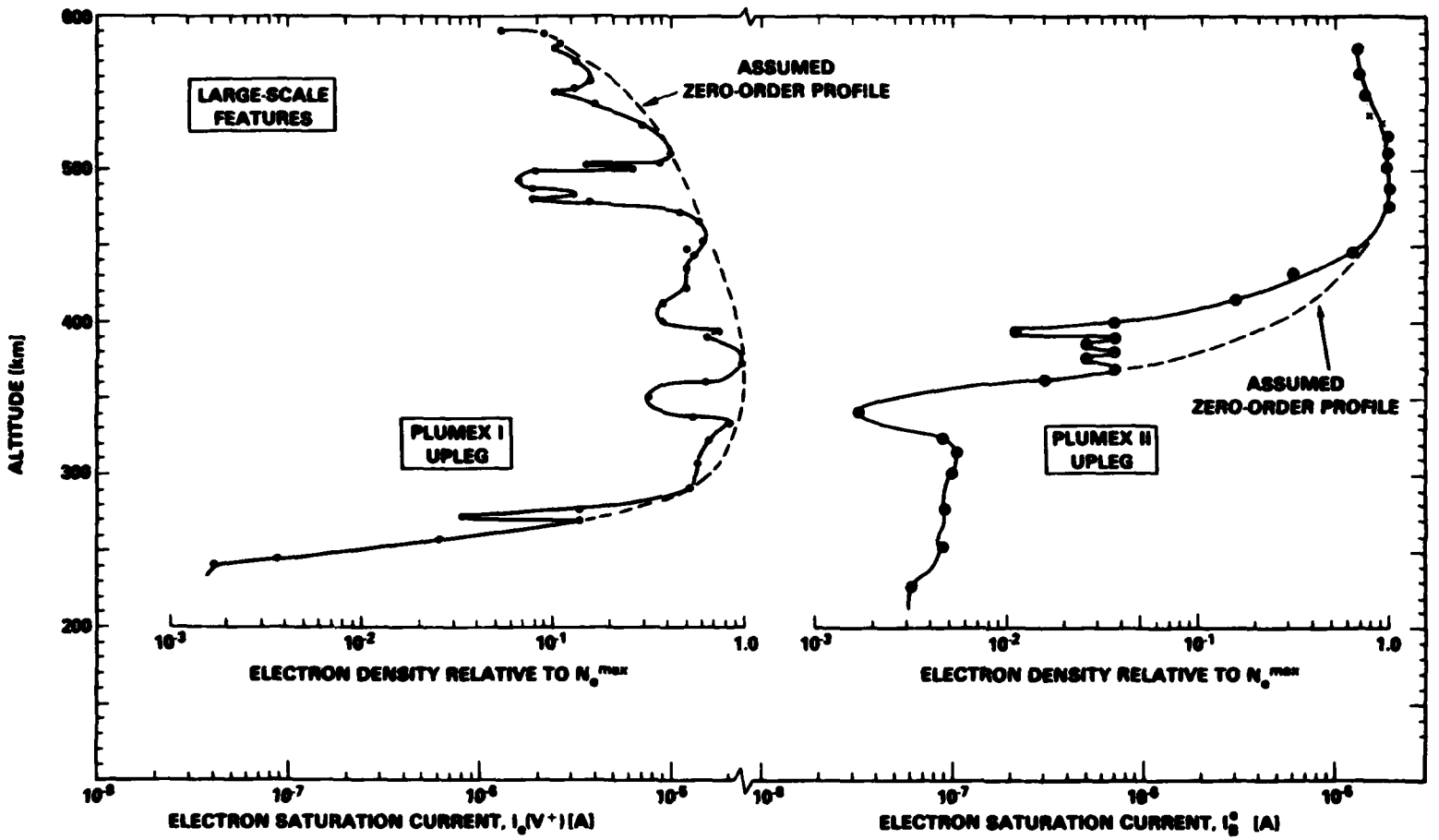

Fig. 4 - Comparison of F-region profiles in PLUMEX I and II.

APPENDIX A

NRL Memorandum Report 4201

PLUMEX I: Coincident Radar and Rocket Observations of Equatorial Spread-F

E. P. SZUSZCZEWICZ

E. O. Hulburt Center for Space Research

R. T. TSUNODA

SRI International
Menlo Park, CA 94075

R. NARCISI

Hanscom Air Force Base
Bedford, MA 01731

J. C. HOLMES

E. O. Hulburt Center for Space Research

March 17, 1980

This work was partially sponsored by the Defense Nuclear Agency under Subtask I25AAXHX640, Communications Effects Experiments, and under contract DNA 001-C-0153.

NAVAL RESEARCH LABORATORY
Washington, D.C.

SECURITY CLASSIFICATION OF THIS PAGE (When Data Entered)

REPORT DOCUMENTATION PAGE

READ INSTRUCTIONS BEFORE COMPLETING FORM

1. REPORT NUMBER: NRL Memorandum Report 4201	2. GOVT ACCESSION NO.
3. RECIPIENT'S CATALOG NUMBER	
4. TITLE (and Subtitle): PLUMEX I: COINCIDENT RADAR AND ROCKET OBSERVATIONS OF EQUATORIAL SPREAD-F	5. TYPE OF REPORT & PERIOD COVERED: Interim report on a continuing DNA problem.
6. PERFORMING ORG. REPORT NUMBER	
7. AUTHOR(s): E. P. Szuszczewicz, R. T. Tsunoda*, R. Narcisi†, and J. C. Holmes	8. CONTRACT OR GRANT NUMBER(s)
9. PERFORMING ORGANIZATION NAME AND ADDRESS: Naval Research Laboratory, Washington, DC 20375	10. PROGRAM ELEMENT, PROJECT, TASK AREA & WORK UNIT NUMBERS: 61153N; RR033-02-44; 71-0949-0-0; DNA Subtask I25AAXHX640
11. CONTROLLING OFFICE NAME AND ADDRESS: Office of Naval Research, Arlington, Virginia 22217	12. REPORT DATE: March 17, 1980
	13. NUMBER OF PAGES: 28
14. MONITORING AGENCY NAME & ADDRESS(if different from Controlling Office)	15. SECURITY CLASS. (of this report): UNCLASSIFIED
	15a. DECLASSIFICATION/DOWNGRADING SCHEDULE

16. DISTRIBUTION STATEMENT (of this Report)

Approved for public release; distribution unlimited.

17. DISTRIBUTION STATEMENT (of the abstract entered in Block 20, if different from Report)

18. SUPPLEMENTARY NOTES

*Present address: SRI International, 333 Ravenwood Ave., Menlo Park, CA 94025.
†Present address: Air Force Geophysics Laboratory, Hanscom Air Force Base, Bedford, MA 01731.
This work was partially sponsored by the Defense Nuclear Agency under Subtask I25AAXHX640, Communications Effects Experiments, and under contract DNA 001-C-0158.

19. KEY WORDS (Continue on reverse side if necessary and identify by block number)

Ionosphere
Electron density
Spread-F
In situ measurements

20. ABSTRACT (Continue on reverse side if necessary and identify by block number)

Coordinated measurements of equatorial spread-F conducted during July 1979 at the Kwajalein Atoll have yielded the first definitive space- and time coincident radar and rocket observations of small scale irregularities and large scale plasma depletions. The results have shown that:

(a) Within a large-scale topside F-layer depletion radar backscatter energy is at a level much lower than that observed on the depletion's topside. The same is true of "in situ" irregularity observations, and

(Continues)

DD FORM 1 JAN 73 1473 EDITION OF 1 NOV 65 IS OBSOLETE
S/N 0102-014-6601

SECURITY CLASSIFICATION OF THIS PAGE (When Data Entered)

20. Abstract (Continued)

(b) Ion composition within a topside depletion can provide signatures of its bottomside source domain and estimates of average maximum vertical drift velocity. For long-lived depletions, molecular-ion signatures (NO^+ and O_2^+) can be lost while bottomside levels of N^+ can be maintained when $[O^+] \approx N_e \gg [NO^+] + [O_2^+]$, and finally,

(c) Large scale fluctuations of O^+ accompanied by a near-constant level of NO^+ and O_2^+ on the bottomside F-layer gradient suggests that neutral atmospheric turbulence is not a major source for bottomside ionospheric plasma irregularities.

PART II
CONTENTS

I. INTRODUCTION

Accumulated information regarding equatorial spread-F phenomena has pointed toward a definite causal relationship between the large scale depletions (also referred to as holes, bite-outs, or bubbles) and range-time-intensity observations of large ionospheric domains with strong radar backscatter returns from the much smaller (meter size) irregularities (called plumes). Woodman and LaHoz (1976) and Kelly, et al. (1976), have suggested that a plume was due to a rising bubble leaving behind a wake of short wavelength irregularities. Another proposal (Szuszczewicz, 1978), arising from considerations of chemistry and transport, suggested that the radar returns originate across the density gradients at the boundaries of large scale depletions. This concept is supported by the work of Ossakow, et al. (1979) where it is inferred that a bubble rising through the F-layer will bifurcate on its topside and produce shorter and shorter wavelength irregularities, either by a cascade or two-step mechanism. Experimental evidence to verify this position has come from an Altair radar experiment (Tsunoda, 1980a) which showed that backscatter maxima tend to occur at altitudes corresponding either to the electron density minima or the upper wall of the plasma depletion. More recently, Tsunoda (1980b) concluded that during the decay phase of meter scale backscatter plumes, the radar returns were maximum on the upper walls of the plasma depletions.

Note: Manuscript submitted February 22, 1980.

Efforts to examine the exact relationship between radar plumes and ionospheric depletions by performing simultaneous "in situ" and ground-based radar observations (Kelly, et al. 1976; Morse, et al. 1977) have been limited to conditions of bottomside spread-F and required extrapolations in space and time to establish correlations. As expected for bottomside spread-F, the "in situ" probes only observed plasma fluctuations along the portion of the trajectory below the F-layer peak density while the ionosphere above the peak was quite smooth.

The ion composition within the depletions has also been the subject of a number of investigations. Typically, satellite mass spectrometric observations (Brinton et al. 1975; McClure et al, 1977; Szuszczewicz, 1978) have shown that the ion composition can be vastly different inside and outside the bite-outs. Fe^+ ions may be enhanced or depleted, with molecular ions usually more abundant inside the bite-out. Brinton et al. (1975) and McClure et al. (1977) have found O^+ depleted by as much as a factor of 10^3 to a concentration below that of NO^+. The molecular ion NO^+ was found to be dominant in the O^+ depleted region, with the bite-outs varying from a few kilometers to tens of kilometers in width. An analysis of the Atmospheric Explorer-C data (Szuszczewicz, 1978) suggested that a given chemical volume on the bottomside F-layer ($[NO^+]$, $[O_2^+] > [O^+]$) could move upward through a stationary neutral atmosphere and

appear at higher altitudes as a bite-out in the local plasma density. As the bottomside F-region plasma cell moved upward, the relative magnitudes of its ionic components would depend on transit time and on altitude through the height distribution of the neutral gases. This model was consistent with the satellite observations as well as the computational work of Scannapieco and Ossakow (1976).

In a continuing effort to understand the detailed relationships involving large scale plasma depletions, meter-size irregularities and associated ion-chemical signatures, a rocket payload instrumented with a plasma diagnostics complement (plasma probes, electric field sensors, mass spectrometer and a two-frequency beacon experiment) was launched into the topside F-region ionosphere above Roi-Namur in the Kwajalein Atoll (4.3° N dip latitude). The investigation was part of a major effort which coordinated rocket and Altair radar observations with bottomside soundings and ground-based photometric measurements of F-region winds. We present here the initial coordinated observations of the radar plumes and the "in situ" measurements of the rocket-borne plasma probes and mass spectrometer.

II. EXPERIMENTAL RESULTS

A. Ionospheric Conditions and Radar Maps

By 2100 hr LT on the night of the rocket launch, ionograms showed that the nominal bottomside of the F-layer had risen to an altitude of 400 km. At that point, the F-

layer began drifting downward with an almost immediate occurrence of spread-F. The downward drifting continued (as did the spread-F) at an approximate average velocity of 10m/sec with the bottomside F-layer having descended to an altitude near 270 km when the rocket was launched (12:31:30 UT on day 198; 00:31:30, 17 July 1979, LT).

Operating at 155.5 Mhz (radar backscatter returns from 1 m ionospheric irregularities) the Altair radar executed consecutive east-west scans in a plane that included the penetration of the rocket's upleg trajectory. Figure 1 presents the contours of constant backscatter strength plotted in 10 dB increments. (For details of the Altair system see Tsunoda et al., 1979). The first panel in Figure 1 shows a backscatter plume just moving out of the radar's eastern-most field of view. That plume, with its highest and most intense backscatter region near 510 km, is connected to backscatter domains extending down to the bottomside of the F-layer. The second panel, with a center scan time 137 seconds later than the first, shows the intense backscatter region further to the east, having drifted there with an approximate west-east velocity of 160m/sec. In the third panel the plume has nearly moved completely out of the radar's field of view and the intense region near 510 km has decayed.

B. Rocket Profile and Comparison with Radar

The rocket payload that was launched into the spread-F conditions depicted in Figure 1 carried a quadrupole ion

mass spectrometer (from the Air Force Geophysics Laboratory) a pair of pulsed plasma probes (from the Naval Research Laboratory), vector electric field sensors (from Utah State University) and a two-frequency beacon experiment (SRI International). The pair of pulsed probes simultaneously tracked ion and electron saturation currents while generating conventional Langmuir probe characteristics (see e.g., Szuszczewicz and Holmes, (1977). Figure 2 displays the upleg measurements of relative electron density as presented by correlated ion and electron saturation currents. The ordinate has a linear scale for time-after-launch with altitude superimposed at 50 second increments. (Because ion and electron saturation currents have significantly different sensitivities to velocity, sheath and magnetic field effects (e.g., Szuszczewicz and Takacs, 1979) data points not corroborated by both polarity currents were attributed to the various aspect sensitivities and therefore were not included in Figure 1. This approach facilitates quick look analysis and establishes credibility in the interpretation of the curves as relative electron density profiles.)

The profile shows that the payload entered the very bottom of the F-layer at $t \tilde{-}$ 103 sec ($Z \tilde{-}$ 240 km). From that point, to an apogee near 590 km, the "in situ" measurements revealed a number of plasma depletions depicted in the figure as regions C, D-E, F-G, H-I, and J-K. The largest depletion was in region H-I where $\Delta N_e/N_e^o \tilde{-}$ 0.85 with a half-

minimum vertical extent approximatley equal to 23 km.

In the regions of the large-scale depletions, the "in situ" measurements also revealed much smaller scale irregularities. The central plot of "irregularity intensity" in Figure 2 identifies the regions of smaller irregularities and attempts to establish a preliminary quantification for their intensity. ("Irregularity intensities" were scaled directly from probe current fluctuations about an estimated mean. As an illustration, the -4.5 to +4.5 irregularity intensity within region C represents a factor of 9 in the largest peak-to-peak fluctuation measured in that region. (If vehicle potential, plasma temperature and ion composition were constant during the irregularity measurements, then $I \propto N_e$.) More quantitative analyses along with power spectral densities will be determined for future publication.) The results show that the most intense irregularities occurred on the bottomside gradient (region C) with corresponding measurements at all other altitudes at a much lower level. We note that the fluctuations in the largest depletion (region H-I) are smaller than those at "C". The data also indicate that the more intense fluctuations occur on positive density gradients (C,D,E, and I).

The payload's upleg trajectory has been superimposed on the radar maps in Figure 1 with domains A through K (and their associated times of observation) identified on

the panel best matched for time coincidence with the radar results. A step-wise comparison of "in situ" irregularity observations (Fig. 2) with the radar maps reveals some interesting correlations:

Point "A" corresponds to the lowest position of the bottomside F-layer, while "B" is midway up the steep bottomside and very near the point of maximum positive density gradient. Region "C" is at the boundary of the third highest backscatter level (30 dB), and appears to represent the mid-phase development of large scale Rayleigh-Taylor turbulence. Observations at "D", "E", "F" and "G" occur along the western "wall" of the plume, and encompass an altitude domain identified with the F-layer peak. Point "G" represents the payload's entry into the large scale depletion centered near 240 sec (490 km) on the upleg trajectory. The payload's transit from "G" to "I" is marked by a positive gradient in backscatter radar energy, with the maximum return occurring on the topside (region "I" and above) of the H-I depletion. Above the large scale depletion, observations "K" and "J" begin to track the western "wall" of the plume in the topside F-region.

C. Ion Composition

O^+ was observed to be the dominant ion component throughout the entire F-region. From points of view focussed on turbulence and transport the chemical constituency of two regions are worthy of note:

In the H-I depletion on the topside F-layer the major observed ion components were $[O^+] \tilde{-} 0.998\ N_e$, $[N^+] \tilde{-} 0.002\ N_e$ and $([NO^+] + [O_2^+]) < 10^{-4} N_e$. In the adjacent domains there was a different distribution of ions, i.e., outside the depletion we found $[O^+] \tilde{-} 0.992\ N_e$, $[N^+] \tilde{-} 0.007\ N_e$ and $([NO^+] + [O_2^+]) < 2\ (10^{-5})\ N_e$, a distribution typical of the zero-order ionosphere at those altitudes.

The ion composition within the H-I depletion suggests that it may have originated at or near the bottomside F-region where $[O^+] \tilde{-} [O^+]_{H-I}$. Such a region exists at 112 sec ($Z \tilde{-} 262$ km) on the upleg trajectory where it was observed that $[NO^+]$ and $[O_2^+]$ were 1-2% of N_e and the $[O^+]/[N^+]$ ratio was nearly identical to that observed in the H-I domain. This points to N^+ as a long-lived tracer ion for bottomside source regions of topside depletions. The fact that the source region levels of NO^+ and O_2^+ have not been preserved in the topside hole results from their losses by dissociative recombination and a simultaneous loss in production by ion-atom interchange and charge exchange reactions since $[N_2]$ and $[O_2]$ decrease markedly with altitude. The longer it takes a bottomside depletion to move upward into the topside F-layer, the more likely the elimination of molecular ion signatures when $[O^+] \tilde{-} N_e > ([NO^+] + [O_2^+])$. In the case of the H-I depletion, a vertical transport time greater than 360 seconds would account for the molecular ion deficiency. (To arrive at this estimate we assumed an instaneous displacement of the bottomside ion composition to the H-I

altitude and calculated that in about 6 minutes the molecular ions would decrease to a concentration less than 5 cm^{-3}.) This time estimate suggests an upper limit of about 600 m/sec for the depletion's average vertical drift velocity, a value which is consistent with the wide range in predicted bubble rise velocities (Ossakow and Chaturvedi, 1978; Ossakow et al., 1979; Anderson and Haerendel, 1979). (While this conclusion is correct in its own right, we note that Altair data prior to that shown in Fig. 1 reveal that the backscatter plume was at the nominal altitude shown in Figure 1 for more than 30 minutes.)

The second region of special note is "C" where it was observed that O^+ followed the intense plasma density fluctuations while the molecular ions NO^+ and O_2^+ (representing @0.5-1.0% N_e) did not. Such a result has a possible explanation in an assumption that requires steady state chemical equilibrium in an O^+ dominant domain. (Molecular ions in region "C" can achieve equilibrium concentrations in less than 10 minutes.) Under this condition, molecular ion concentrations are independent of O^+ and vary only with the scale height of the neutral atmospheric constituents N_2 and O_2. The observations conform to this model with a standard zero-order atmospheric distribution, suggesting that neutral atmospheric turbulence is not a major source for the observed plasma fluctuations on the bottomside F-region.

D. North-South Extent of the Depletions

Figure 3 presents the up- and downleg profiles of relative electron density as measured by "in situ" probe electron-saturation currents. (The integrity of the downleg profile was established by the same procedure utilized in Figure 2.) A comparison of the profiles shows very good agreement in the two observations of plasma depletions. Attention is directed to the large scale depletion of the topside (region H-I):

The up- and downleg measurements of the large topside hole were separated in time by approximately 340 seconds and in range by 112 km. During this 340 second interval Altair radar measurements of plume movement showed an average easterly drift at a 160 m/sec rate resulting in a total eastward displacement of 54 km. Adding 14 km to account for depletion alignment along the magnetic meridian (9^{o}E of true azimuth) yields a calculated total E-W displacement of 68 km between the times of the two rocket observations of the hole. During this time interval the payload had an eastward range velocity approximately equal to 215 m/sec, resulting in an east-west separation in the up- and downleg observations of region H-I equal to 73 km. From this we can conclude near-perfect up- and downleg targeting of the hole. The agreement in the two observations of the H-I domain therefore suggests that the depletion is aligned with the magnetic field for at least 112 km. (Parallel arguments dealing with the depletion at $(t,Z) \tilde{=}$ (153s, 350 km) would suggest a field alignment at least as great as 163 km, while the

radar observations of Tsunoda [1980b] showed plasma bubble alignment can extend to 1100 km.)

III. COMMENTS AND CONCLUSIONS

Space- and time coincident measurements of equatorial spread-F conducted during July 1979 at the Kwajalein Atoll have yielded the first definitive observations of small scale irregularities (@1 meter) and large scale plasma depletions as measured independently throughout the F-region by ground-based radar and "in situ" plasma instrumentation. Preliminary analysis of the results leads to the following comments and conclusions:

(a) Within a large-scale, decay-phase, topside F-layer depletion where "in situ" irregularities were reduced (compared with the depletion's topside wall), the radar's backscatter energy was also reduced (compared with the topside wall). This result suggests the co-location of maximum radar returns with the upper regions of a depletion (its topside wall and above) and not with the depletion minimum or bottomside wall.

(b) The "in situ" measurements established field alignment of large scale depletions to distances at least as great as 163 km. This result supports the topside sounder data of Dyson and Benson (1968), the airglow observations of Weber et al., (1978), the recent radar measurements of Tsunoda (1980 a,b) and the assumption of depleted flux tubes in the theoretical considerations of Anderson and Haerendel (1979).

(c) Ion composition measurements within a topside depletion showed little evidence of bottomside molecular tracer ions (i.e., NO^+ and O_2^+). This result points to the requirement for rapid bubble rise velocities and/or low plasma densities ($N_e << 10^4$ cm^{-3}) within the hole if the bottomside molecular ion composition is to be maintained as bubbles drift upward through the F-region (Szuszczewicz, 1978). However, the measurements did reveal N^+ as a longer lived tracer ion. This helped identify the lower altitude source region to be on the bottomside F-layer gradient.

(d) Strong irregularities on the bottomside F-region gradient showed O^+ following large scale density fluctuations while the molecular ions NO^+ and O_2^+ were relatively constant. Preliminary analysis of this result suggests chemical equilibrium and eliminates neutral atmospheric turbulence as a major source of the bottomside plasma irregularities.

(e) An estimate of bubble rise velocity was arrived at by preliminary ion chemical analysis of composition within the hole. The analysis suggests an upper limit of 600 m/sec for the average vertical velocity of an 85% depleted domain (85% on the topside, 100% at the F-peak) as it drifted upward from its bottomside source region near 260 km to the topside F-layer at 490 km. This upper limit is consistent with the wide range in predicted values (Ossakow and Chaturvedi, 1978; Ossakow et al., 1979; Anderson and Haerendel, 1979).

ACKNOWLEDGMENTS

Support for the plasma probe analysis was provided by the Defense Nuclear Agency (DNA) under Subtask Code I25AAXHX640, Communications Effects Experiments. The Altair radar analysis was also supported by DNA under contract DNA 001-C-0153. Support for the ion composition measurements was supplied mostly by the Air Force Office of Scientific Research under Task 2310-G3 and partially by DNA under Subtask I25AAXHX640, Work Unit 06. We also wish to acknowledge the dedicated technical support of E. Trzcinski, G. Federico, L. Wlodyka, L. Kegley and D. Walker, who independently and as a team contributed significantly to the successful execution of the rocket-borne plasma probe and mass spectrometer experiments. Development of the plasma probe technique was provided by the Office of Naval Research under Work Unit A02-11.11 (71-0949-0-0), Ionospheric and Stratospheric Interactions, Task Area RR 043-02-44.

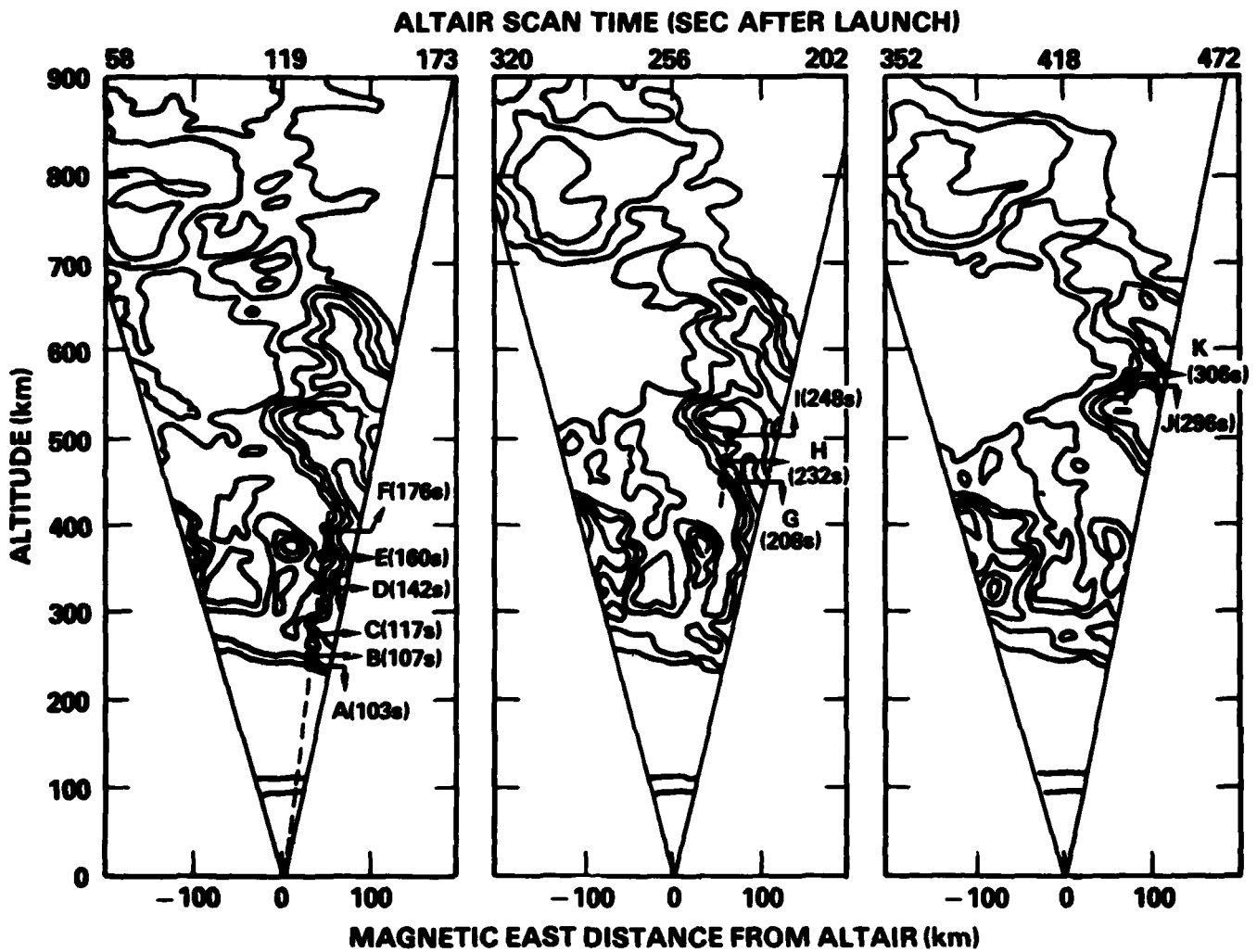

Fig. 1 — Backscatter intensity contour maps (contours are in 10 dB increments) with superposition of the rocket trajectory. The times identified with observations "A" through "K" are included for a more complete representation of temporal correlation with the successive radar scans.

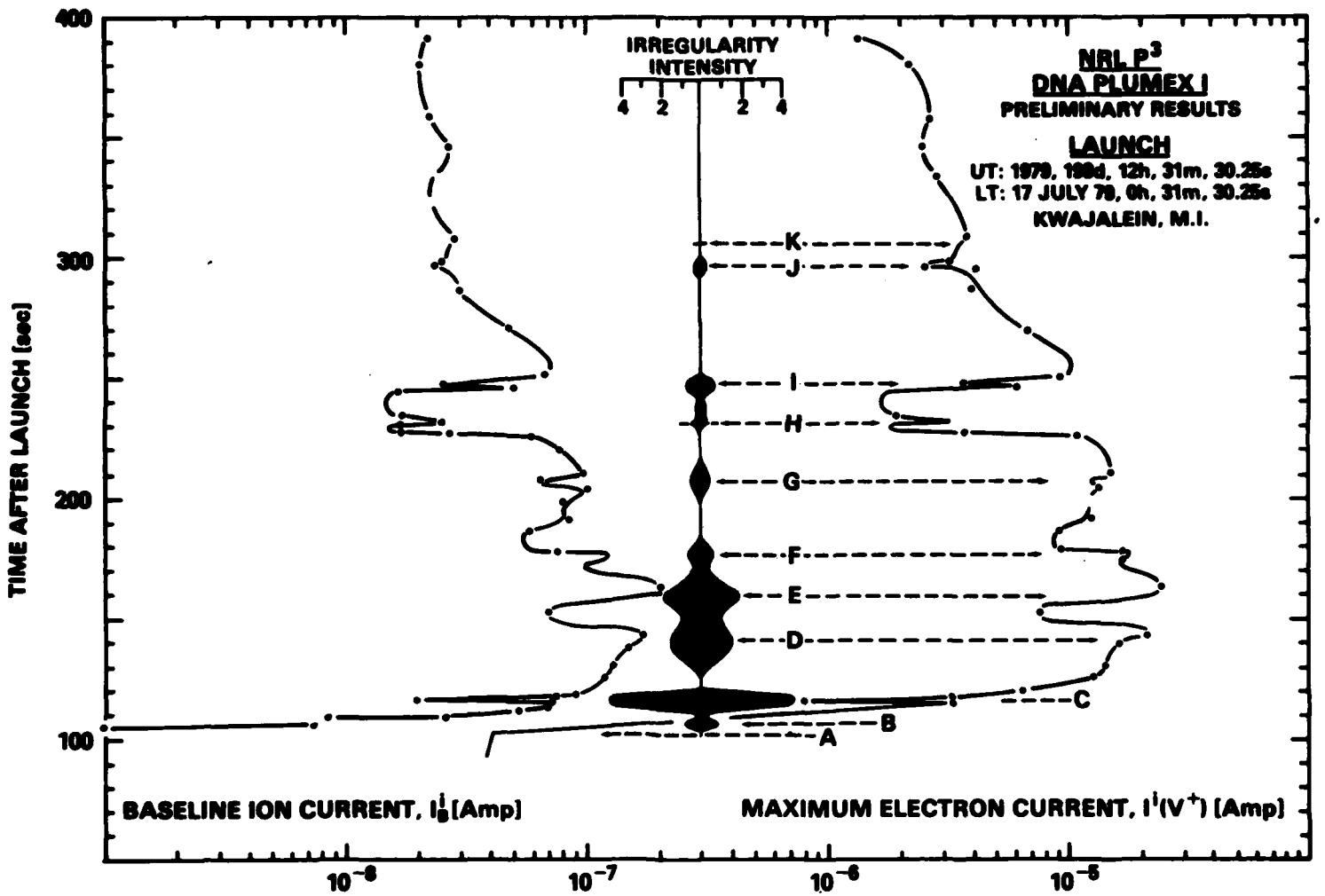

Fig. 2— Relative electron density profile as measured simultaneously by ion and electron saturation probe currents collected on the upleg trajectory. The "irregularity intensity" provides an approximate measure of smaller scale structure as scaled from analog strip chart records of probe current fluctuations.

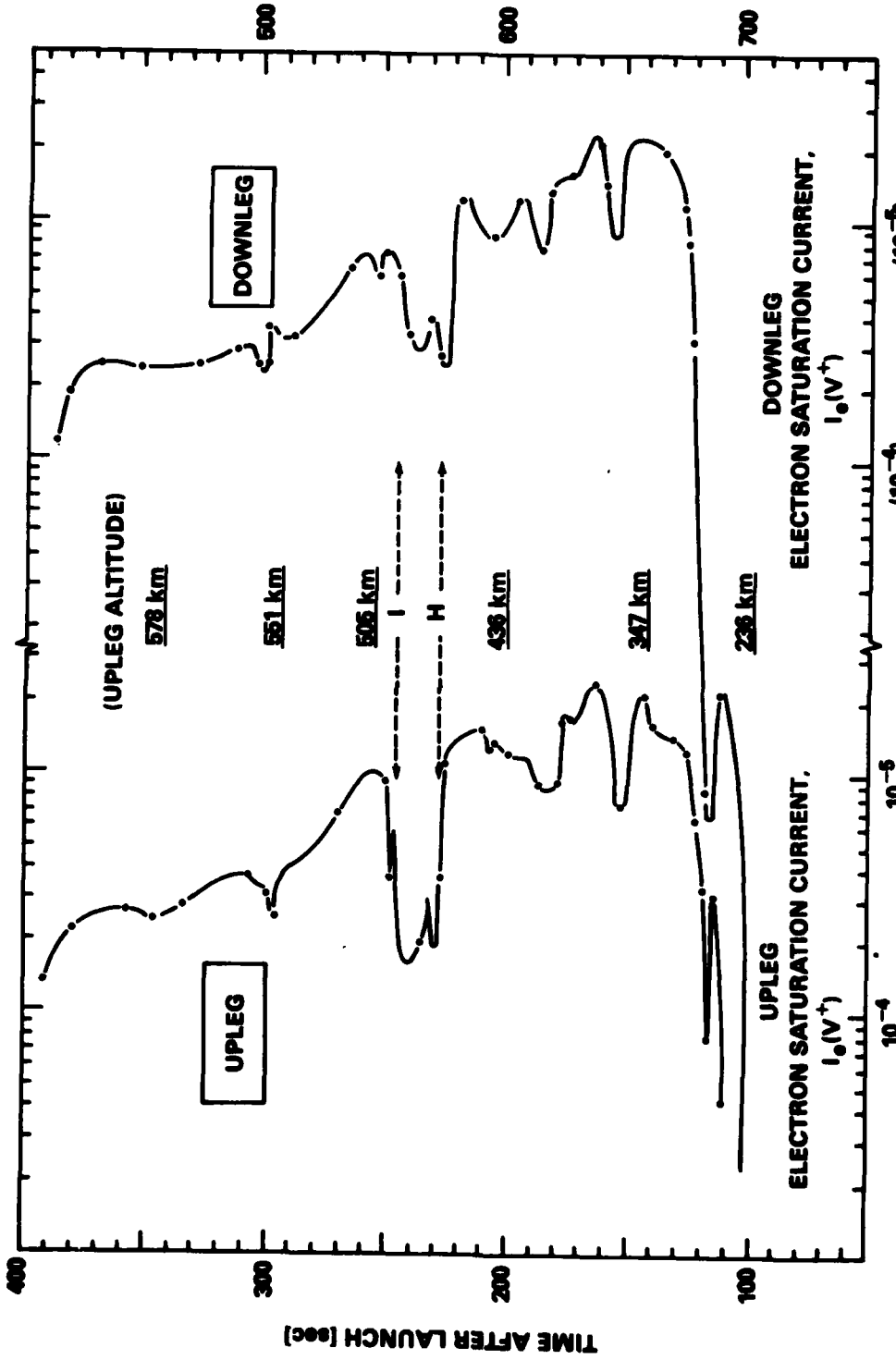

Fig. 3— Comparison of up- and downleg plasma profiles

REFERENCES

Anderson, D.N., and G. Haerendel, "The motion of depleted plasma regions in the equatorial ionosphere," J. Geophys. Res., 84, 4251, 1979.

Brinton, H.C., H. G. Mayr, and G. P. Newton, "Ion composition in the nighttime equatorial F-region: Implications for chemistry and dynamics" (abstract), Eos Trans. AGU, 56, 1038, 1975.

Dyson, P.L., and R.F. Benson, "Topside sounder observations of equatorial bubbles," Geophys. Res. Lett. 5, 795, 1978.

Kelly, M.C., G. Haerendel, H. Kappler, A. Valenzuela, B.B. Balsley, D.A. Carter, W.L. Ecklund, C.W. Carson, B. Hausler, and R. Torbert, "Evidence for a Rayleigh-Taylor type instability and upwelling of depleted density regions during equatorial spread F," Geophys. Res. Lett., 3, 448, 1976.

McClure, J.P., W.B. Hanson, and J.H. Hoffman, "Plasma bubbles and irregularities in the equatorial ionosphere," J. Geophys. Res., 82, 2650, 1977.

Morse, F. A., B.C. Edgar, H.C. Koons, C.J. Rice, W.J. Heikkila, J.H. Hoffman, B.A. Tinsley, J.D. Winningham, A.B. Christensen, R.F. Woodman, J. Pomalaza, and N.R. Teizeira, "Equion, and equatorial ionospheric irregularity experiment," J. Geophys. Res., 82, 578, 1977.

Ossakow, S. L., and P.K. Chaturvedi, "Morphological studies of rising equatorial spread-F bubbles," J. Geophys. Res., 83, 2084, 1978.

Ossakow, S.L., S.T. Zalesak, B.E. McDonald, and P.K. Chaturvedi, "Nonlinear equatorial spread F: Dependence on altitude of the F peak and bottomside background electron density scale length," J.Geophys. Res. 84, 17, 1979.

Scannapieco, A.J., and S.L. Ossakow, "Nonlinear equatorial spread F," Geophys. Res. Lett., 3, 451, 1976.

Szuszczewicz, E.P. and J.C. Holmes, "Observations of electron temperature gradients in mid-latitude E_s layers," J. Geophys. Res., 82, 5073, 1977.

Szuszczewicz, E.P., "Ionospheric holes and equatorial spread-F: Chemistry and transport," J. Geophys. Res. 83, 2665, 1978.

Szuszczewicz, E.P., and P.Z. Takacs, "Magnetosheath effects on cylindrical Langmuir probes," Phys. Fluids 22, 2424, 1979.

Tsunoda, R.T., M.J. Baron, J. Owen and D.M. Towle, "Altair: An Incoherent scatter radar for equatorial spread-F studies," Radio Sci., 14, in press, 1979.

Tsunoda, R.T., "On the spatial relationship of 1-m equatorial spread-F irregularities and plasma bubbles," J. Geophys. Res. 85, (in press, 1980a).

Tsunoda, R.T., "Magnetic-field-aligned characteristics of plasma bubbles in the nighttime equatorial ionosphere," J. Atmos. Terr. Phys. (submitted, January 1980).

Weber, E.J., J. Buchau, R.H. Eather, and S.B. Mende, "North-south aligned equatorial airglow depletions," J. Geophys. Res., 83, 712, 1978.

Woodman, R.F., and C. LaHoz, "Radar observations of F region equatorial irregularities," J. Geophys. Res., 81, 5447, 1976.

APPENDIX B

NRL Memorandum Report 4289

Equatorial Spread F: "In Situ" Measurements of Electron Density Temperature and Density Fluctuation Power Spectra

E.P. SZUSZCZEWICZ AND J.C. HOLMES

Ionospheric Diagnostics Section
Space Science Division

August 25, 1980

This research was sponsored by the Defense Nuclear Agency under subtask I25AAXHX640, work unit 12 (Plasma Probes), and work unit title, "Nuclear Weapons and Ionospheric Effects."

NAVAL RESEARCH LABORATORY
Washington, D.C.

SECURITY CLASSIFICATION OF THIS PAGE (When Data Entered)

REPORT DOCUMENTATION PAGE		READ INSTRUCTIONS BEFORE COMPLETING FORM
1. REPORT NUMBER NRL Memorandum Report 4289	2. GOVT ACCESSION NO.	3. RECIPIENT'S CATALOG NUMBER
4. TITLE (and Subtitle) EQUATORIAL SPREAD F: "IN SITU" MEASUREMENTS OF ELECTRON DENSITY TEMPERATURE AND DENSITY FLUCTUATION POWER SPECTRA		5. TYPE OF REPORT & PERIOD COVERED Interim report on a continuing DNA problem. 6. PERFORMING ORG. REPORT NUMBER
7. AUTHOR(s) E.P. Szuszczewicz and J.C. Holmes		8. CONTRACT OR GRANT NUMBER(s)
9. PERFORMING ORGANIZATION NAME AND ADDRESS Naval Research Laboratory Washington, D.C. 20375		10. PROGRAM ELEMENT, PROJECT, TASK AREA & WORK UNIT NUMBERS 62710H; 71-0950-0-0
11. CONTROLLING OFFICE NAME AND ADDRESS Defense Nuclear Agency Washington, D.C. 20305		12. REPORT DATE August 25, 1980 13. NUMBER OF PAGES 35
14. MONITORING AGENCY NAME & ADDRESS(if different from Controlling Office)		15. SECURITY CLASS. (of this report) UNCLASSIFIED 15a. DECLASSIFICATION/DOWNGRADING SCHEDULE

16. DISTRIBUTION STATEMENT (of this Report)

Approved for public release; distribution unlimited.

17. DISTRIBUTION STATEMENT (of the abstract entered in Block 20, if different from Report)

18. SUPPLEMENTARY NOTES

This research was sponsored by the Defense Nuclear Agency under subtask I25AAXHX640, work unit 12 (Plasma Probes), and work unit title, "Nuclear Weapons and Ionospheric Effects."

19. KEY WORDS (Continue on reverse side if necessary and identify by block number)

Absolute density
Temperature
Density fluctuation power spectra
In Situ irregularities

20. ABSTRACT (Continue on reverse side if necessary and identify by block number)

The NRL pulsed plasma probe experiment was successfully flown on each of the two PLUMEX rockets during July 1979. The experiment provided direct measurements of absolute density N_e, temperature T_e and density fluctuation power spectra with a maximum Nyquist frequency of 1 KHz (1 meter resolution at a 1 km/sec rocket velocity). In the first operation, a number of major depletions ($\Delta N_e/N_e^0 \lesssim 90\%$) were distributed throughout the F-region, from its bottomside gradient centered near 260 km,

(Continues)

DD FORM 1 JAN 73 1473 EDITION OF 1 NOV 65 IS OBSOLETE
S/N 0102-LF-014-6601

SECURITY CLASSIFICATION OF THIS PAGE (When Data Entered)

20. Abstract (Continued)

through the F-peak, to a topside altitude of 500 km. The F-peak was at 375 km, with N_e^{max} = 1.3 (10^6) cm^{-3} (± 10%). The electron energy distribution was characterized by T_e = 1350 (± 250)°K with no obvious signatures of energy redistribution in and around the depletions. The most intense "in situ" irregularities occurred on the bottomside ledge where gradient scale lengths were found to vary between 2 and 25 km. The power spectral density in this region of intense irregularities on the bottomside was dominated by a $k^{-2.5}$ power law over the intermediate wavelength domain k = 2π/1 km to k = 2π/2.5 m. This result supports the role of the collisional Rayleigh-Taylor instability in generating intermediate wavelength irregularities during the occurrence of equatorial spread-F.

PART III
CONTENTS

EQUATORIAL SPREAD F: "IN SITU" MEASUREMENTS OF ELECTRON DENSITY TEMPERATURE AND DENSITY FLUCTUATION POWER SPECTRA

I. INTRODUCTION

The DNA/PLUMEX rocket payloads launched into the equatorial ionosphere during the July 1979 campaign carried a plasma diagnostics complement that included a quadrupole ion mass spectrometer, a pair of pulsed plasma probes, vector electric field sensors and a four-frequency beacon. The pair of pulsed plasma probes not only provided simultaneous measurements of electron density N_e, temperature T_e, and density fluctuation power spectra $P_n(k)$, but also provided the capability for a running measurement of relative variations in mean ion mass $\langle M_i \rangle$.

The measurements of N_e and T_e form the basic information on the laminar condition of the ionosphere, allowing for the determination of the ionospheric plasma response to varying geophysical conditions (solar and magnetic activity, winds, gravity waves, etc.) and the detection of triggering mechanisms (e.g., steep density gradients in N_e) for ionospheric irregularities.

The measurements of $\delta N_e (\rightarrow P_n(k))$ yield important test information for signal channel models as well as candidate instability mechanisms (e.g., collisional drift modes, $\bar{E} \times \bar{B}$ and Rayleigh-Taylor) which might be active in the ionospheric plasma.

In this paper we describe the experimental technique, payload configuration, launch scenerios and present additional experimental results which complement companion papers[1,2].

Manuscript submitted June 18, 1980

II. TECHNICAL OVERVIEW

Introduction. The pulsed plasma probe technique (P^3 is the designated acronym) is a unique diagnostic tool capable of high spatial and temporal resolution of plasma parameters. The instrument is a Langmuir-type probe using a special electronic procedure for generating the current-voltage characteristic[3,4]. The result is greatly improved reliability and expanded versatility in Langmuir probe measurements. As a diagnostic tool, the P^3 technique reduces commonly found distortions in derived electron densities and energy distribution functions. A unique feature of the technique is its ability to measure simultaneously the electron temperature, density, and the density fluctuation power spectrum. Successful applications of the P^3 technique include not only rocket but also satellite [5,6] and laboratory beam-plasma studies[7] of turbulent charged-particle environments.

Figure 1 shows two types of probe operation. Figure 1(A) depicts a linear sawtooth sweep voltage which represents the conventional approach to Langmuir probe operation wherein some form of continuous voltage sweep is applied between voltage limits V_- and V_+. Fig. 1(B) shows the pulse-modulated sweep which has been utilized with P^3. The voltage pulses which follow the sawtooth envelope generate the probe's current-voltage characteristic. During the interpulse period, at constant voltage V_B, the collected probe current I_B provides a direct measure of variations in the probe-plasma system. The pulse duty-cycle is short so that the

probe rests at its baseline potential V_B for a period much longer than the pulse width. Fig. 2 shows pulse and baseline durations identified as τ_{on} and τ_B, respectively. So that sweep voltage transients will not affect the value of probe current, the probe current is sampled at the termination of subinterval τ_i within the sweep pulse and at the center of the baseline interval τ_B.

With τ_{on} much shorter than either τ_B or the time constant of the probe surface contamination layer[4], the pulse procedure will maintain the surface condition and associated voltage drop at a more nearly constant level than when using a continuous, slowly-varying sweep voltage. The resulting current-voltage characteristic can then be unfolded from the plasma density fluctuations (δI_B) so that the electron temperature and density are determined uniquely. In addition, the I_B-values provide the raw data from which density fluctuation power spectra are determined.

Payload configuration and P^3 characteristics. A pair of pulsed probes were diametrically extended from the forward end of the rocket payload (Fig. 3). The sensing elements constructed from tungsten wire, were isolated from their extension booms by coaxial guard electrodes driven at the same potential as the probes themselves. One of the probes, defined as the I-probe, operated with $V_B \sim$ -1v, yielding net ion baseline current I_B^i. The other probe, defined as the E-probe, operated with $V_B \sim$ + 2v, yielding net electron baseline current I_B^e. Both probes generated

complete current-voltage characteristics in $\tau_s \approx 400$ msec, yielding absolute values of N_e and T_e at an approximate 2.5 Hz rate. Maximum I_B sampling occurred at 2048 Hz, resulting in 0.5 meter spatial resolution for relative electron density fluctuations at a vehicle velocity of 1 km/sec.

Probe electrometers were set to operate over a dynamic range extending from $4(10^{-10})$ to 2.5 (10^{-4}) amperes, with automatic switching over 8 ranges maintaining 9 bit accuracy for all anticipated ionospheric conditions. The automatic ranging is best illustrated in Figure 4, an actual in-flight analog record of telemetry channel outputs for the probe currents and applied voltages, the roll magnetometer for magnetic aspect determinations, and pitch, yaw and roll monitors on the ACS jets. The data sample presented in Figure 4 was collected when the payload was 55 seconds into flight while the probe electrometers were being driven through a load resistor for calibration. The probes' operation alternated between a fixed-bias mode and a pulsed-sweep mode, with absolute currents determined by a simple algorithm which coupled the switching 0-5 v TM signal on PCM channel 26-1 with the sweep current range monitor on channel 27-1. The record format in Fig. 4 helped provide field-estimates of density profiles without distortions of magnetic aspect sensitivities and attitude control jets.

III. RESULTS

Density profiles and irregularity structures. By 9 P.M. (LT) on the night of the first rocket launch (PLUMEX I) the bottomside of the F-region had risen to an approximate

altitude of 400 km. The F-region then began a downward drift with a simultaneous onset of spread-F. The downward drifting and spread-F conditions continued, and when the bottomside F-layer had descended to an altitude below 300 km, the rocket was launched (12:31:30 UT on day 198; 00:31:30, 17 July 1979, LT).

Figure 5 displays the upleg measurements of relative electron density as presented by correlated ion- (I_B^i) and electron- saturation $I_e^i(V^+)$ currents. The ordinate has a linear scale for time-after-launch with altitude superimposed at 50 second increments. Because ion and electron saturation currents have significantly different sensitivities to velocity, sheath and magnetic field effects[8], variations in I_B^i and $I_e^i(V^+)$ not mutually corroborated were attributed to the various aspect sensitivities and excluded from Figure 5. This approach facilitated analysis, reduced computer time, and established credibility in the interpretation of the curves as relative electron density profiles.

The results in Figure 5 show that a number of major depletions ($\Delta N_e/N_e^o \lesssim 0.9$) were distributed throughout the F-region. Each of the large scale depletions (identified alphabetically) has its own distribution of irregularities, illustrated in Fig. 6 by the expanded view of regions C, D, H and I. It is clear that "C" is not a single narrow bite-out but a collection of rather large irregular structures

extending over a total altitude domain of about 12 km. (Vehicle velocity in region C was 2.4 km/sec.) To develop a quantitative view of irregularity fluctuations observed in the F-region, continuous linear detrends were executed throughout the entire upleg trajectory. The variations about those linear detrends were then plotted in Figure 5 as "Irregularity Intensity", with a maximum relative scale of $\pm$ 4. A fluctuation as great as $\pm$ 4 approximately represents a $\pm$ 80% fluctuation about the linear detrend. (Correlation of these results with macroscale gradients and Altair backscatter contours are discussed in a companion paper[1].

Absolute density and temperature. Absolute values of electron density and temperature were determined by conventional analyses of Langmuir probe characteristics[9] with appropriate care to eliminate perturbing effects of surface contamination[4], density fluctuations[3,10] and magnetic field effects[8]. Analysis of approximately 25 characteristics were executed over the F-layer from 340-560 km. In each case a conversion coefficient $a \equiv N_e\ [cm^{-3}]/I_e(V^+)$ was determined so that the $I_e(V^+)$ profile in Figure 5 could be directly scaled to absolute electron densities. This procedure yielded $a = (5.5 \pm 0.5)\ 10^{10}$ electrons $cm^{-3}A^{-1}$.

The upleg profile has been reconstructed in Figure 7 with relative and absolute electron density plotted as a function of altitude. The result shows the F-peak at 375 km, with a maximum density of 1.3 $(10^6)cm^{-3}$ ($\pm$ 10%).

Analysis of the retarding-field region of the same set of current-voltage characteristics yielded $T_e = (1350 \pm 250)^{\circ}K$, with no obvious signatures of electron energy redistribution in and around the depletions.

Intermediate wavelength power spectra. The pulsed probe data provided an excellent opportunity for comparison with the numerical simulations[11] of the collisional Rayleigh-Taylor (R-T) instability at intermediate wavelengths. Attention is focused on the bottomside F-layer gradient and region C, which is believed representative of the mid-phase development of the R-T process[1]. Typically, computer simulations employ several values for the zero-order gradient scale length

$$L = \left(\frac{1}{N_e^o} \frac{dN_e^o}{dy} \right)^{-1}$$

and initialize the code with some two-dimensional perturbation superimposed. In the work of Keskinen, et al.[11] L was selected at 5, 10 and 15 km and the perturbation took the form [12]

$$\frac{\delta N_e(x,y,t=0)}{N_e^o} = (10^{-4}) \text{ Sin } (k_y\, y) \text{ Cos } (k_x\, x) + 2(10^{-6}) \text{ Sin } (2k_y\, y)$$

with k_x and k_y being the horizontal and vertical wavenumbers, respectively. Both k_x and k_y were set equal to $2\pi/960$ m in the simulation. In addition, the computation assumed that L was centered at 300 km.

Under actual conditions encountered in PLUMEX I (Fig 7), the bottomside F-layer gradient extended from 240 to 290 km. The question of gradient scale length can be studied in Figure 8 where it is shown that the bottomside gradient (encompassed in the 105-125 sec time frame) is not characterized by a single value of L. In region "C" (114s $\lesssim$ t $\lesssim$ 122s) L is seen to vary between 2 and 10 km, whereas adjacent domains (110s $\leq$ t $\leq$ 113s and 122s $\leq$ t < 126s) can be characterized by L = 25 km. We would suggest that the adjacent domains are representative of the zero-order gradient scale length and that L = 25 km would be a more appropriate value in the numerical simulation.

In any event, computer simulations[11] with L = 5, 10 and 15 km showed that linearly unstable modes saturate by non-linear generation of vertical modes. The results yield one-dimensional power laws (horizontal and vertical) that vary with a spectral index ($\equiv$ n in $P_{N_e} \propto k^{-n}$) between 2.0 and 2.5. To explore this result within the context of region "C", power spectral analyses were conducted over sliding intervals of 2.4 km. The results, presented in Figure 9, show that the dominant behavior is $k^{-2.5}$ over the range k = 2π/1km to k = 2π/25m. The $k^{-1.85}$ behavior at t = 116.001 sec is a result of the very sharp density gradient (see region "C" Fig. 6) encompassed by the domain of the spectral analysis.

In general we would conclude that our results support the numerical simulations of Keskinen, et al.[11]. We do

point out however that a spectral index variation from 2 to 2.5 is a rather broad domain. Further testing of this support can be achieved with an L = 25 km simulation and a downward drifting F-layer model that is more in keeping with the actual experimental conditions. The F-layer time-history can be important since unstable modes appear to require times in excess of 4,000 seconds to saturate...a time during which the F-layer encountered in PLUMEX I drifted downward in excess of 40 km.

IV. SUMMARY

In each of the two rocket operations (PLUMEX I & II) conducted at the Kwajalein Atoll during July 1979, the NRL pulsed plasma probe performed flawlessly. General results concerning coordinated rocket and radar measurements of small and large scale irregularities have been discussed in companion papers[1,2]. Complementary results developed here include:

(a) In PLUMEX I a number of major depletions ($\Delta N_e/N_e^o \lesssim$ 90%) were distributed throughout the F-region, from the bottom-side gradient centered near 260 km, through the F-peak, to a topside altitude of 500 km. The most intense "in situ" irregularities occurred on the bottomside ledge where gradient scale lengths were found to vary between 2 and 25 km. The power spectral density in this region of intense irregularities on the bottomside was dominated by a $k^{-2.5}$ power law over the intermediate wavelength domain k = 2π/1km to k = 2π/2.5m. The experimental conditions were reasonably matched to the

numerical simulations of Keskinen et al.[11], and a comparison of the two resulted in general agreement.

(b) In PLUMEX I, the F-peak was at 375 km, with N_e^{max} = 1.3 (10^6) cm^{-3} ($\pm$ 10%). The electron energy distribution was characterized by T_e = (1350 $\pm$ 250)°K with no obvious signatures of energy redistribution in and around the depletions.

ACKNOWLEDGMENTS

This work was supported by the Defense Nuclear Agency under Subtask Code I25AAXHX640, Communications Effects Experiments (Plasma Probes). We wish to thank L. Kegley for his dedication in every phase of instrument development from design through field operations. We also extend our thanks to Dr. C. S. Lin for his diligence and commitment to the task of data reduction and analysis.

REFERENCES

1. Szuszczewicz, E.P., R.T. Tsunoda, R. Narcisi and J.C. Holmes, "PLUMEX I: Coincident radar and rocket observations of equatorial spread-F," DNA Report ,1980; also published in Geophys. Res. Lett. (in press,July 1980).
2. Szuszczewicz, E.P., R.T. Tsunoda, R. Narcisi and J.C. Holmes, "PLUMEX II: Coincident radar and rocket observations of equatorial spread-F," DNA Report, 1980; also published as NRL Memorandum Report (in press 1980).
3. Holmes, J.C. and E.P. Szuszczewicz, "A versatile plasma probe," Rev. Sci. Instr. 46, 592 (1975).
4. Szuszczewicz, E.P. and J.C. Holmes, "Surface contamination of active electrodes in plasmas: Distortion of conventional Langmuir probe measurements," J. Appl. Phys. 46, 5134 (1975).
5. Szuszczewicz, E.P., J.C. Holmes and D.N. Walker, "On the probing of ion and electron irregularity spectra." EOS 60, 339 (April 1980).
6. Singh, M., E.P. Szuszczewicz and J.C. Holmes, "High resolution measurements of equatorial F-region irregularities," EOS 61, 314 (April 1980).
7. Szuszczewicz, E.P., J.C. Holmes, and D.N. Walker, "Plasma diffusion in a space-simulation beam-plasma-discharge", Geophys. Res. Lett. 6, No. 3 (1979).
8. Szuszczewicz, E.P. and P.Z. Takacs, "Magnetosheath effects on cylindrical Langmuir probes," Phys. Fluids 22, 2424 (1979).
9. Chen, F.F., "Electrical probes," in Plasma Diagnostic Techniques, edited by R.H. Huddlestone and S.L. Leonard (Academic, New York, 1965), p. 113.

10. Szuszczewicz, E.P. and J.C. Holmes, "Observations of electron temperature gradients in mid-latitude E_s layers," J. Geophys. Res., 82, 5073, 1977.

11. Keskinen, M.J., S.L. Ossakow and P. K. Chaturvedi, "Preliminary report on numerical simulations of intermediate wavelength collisional Rayleigh-Taylor instability in equatorial spread-F," J. Geophys. Res. 85, 1775 (1980).

12. Chaturvedi, P.K., and S.L. Ossakow, "Nonlinear theory of the collisional Rayleigh-Taylor instability in equatorial spread-F," Geophys. Res. Lett. 4, 558 (1977).

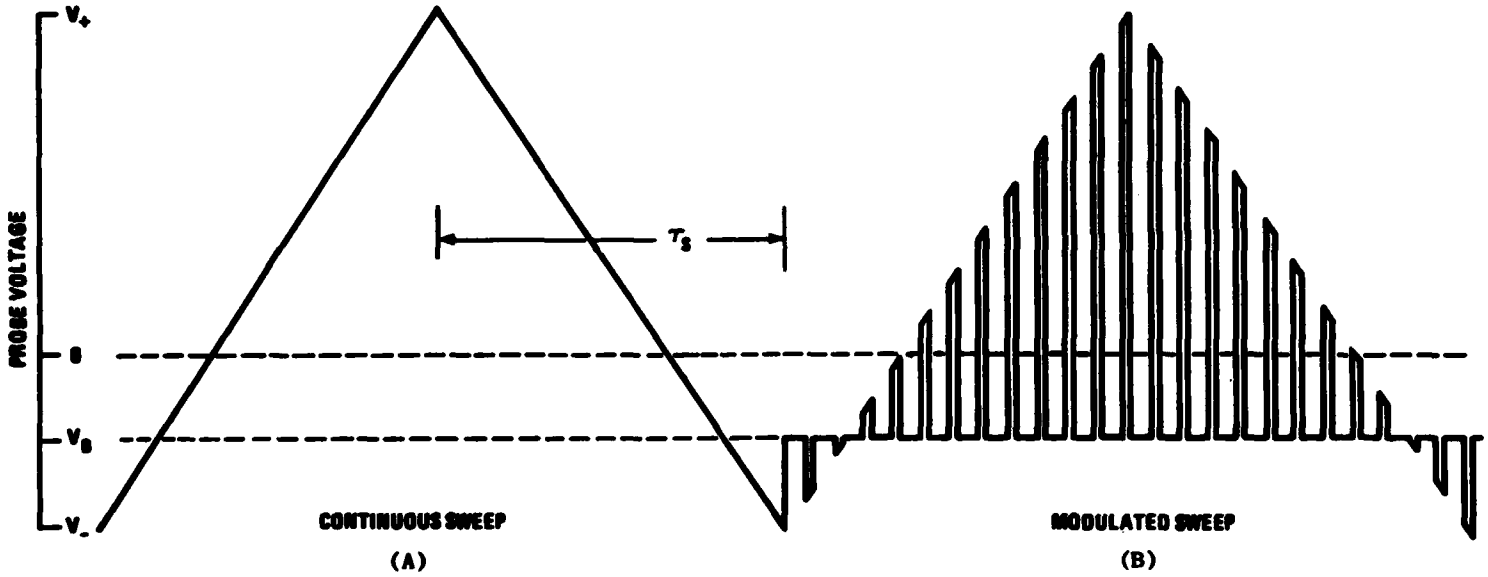

Fig. 1 — Continuous and pulsed modes of probe operation. (A) represents the conventional approach, while (B) shows the modulated sweep utilized in the P^3 technique.

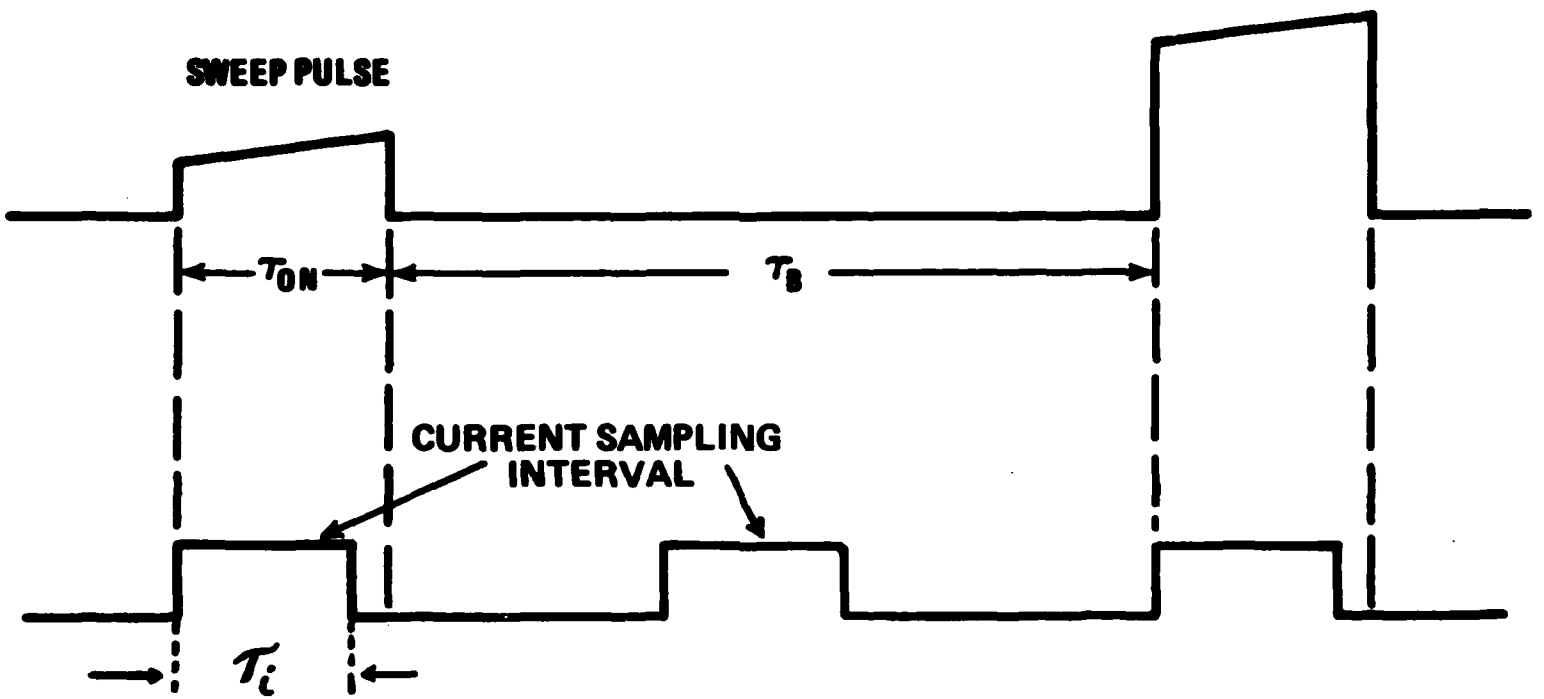

Fig. 2 — The sweep pulses (Fig. 1) shown on an expanded scale to illustrate the probe-current sampling intervals

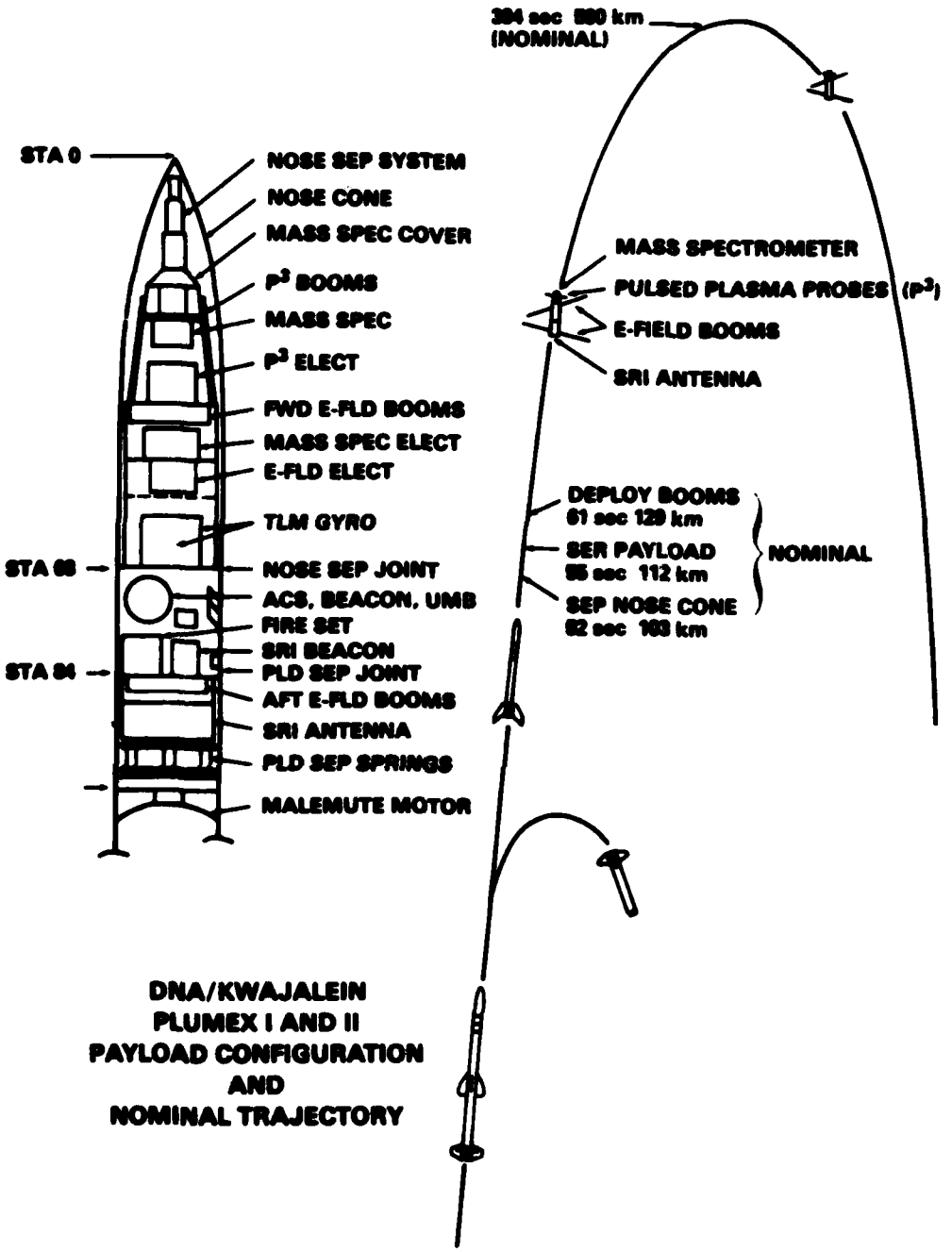

Fig. 3 — PLUMEX payload configuration and nominal trajectory. (This figure has been adapted from a Sandia report.)

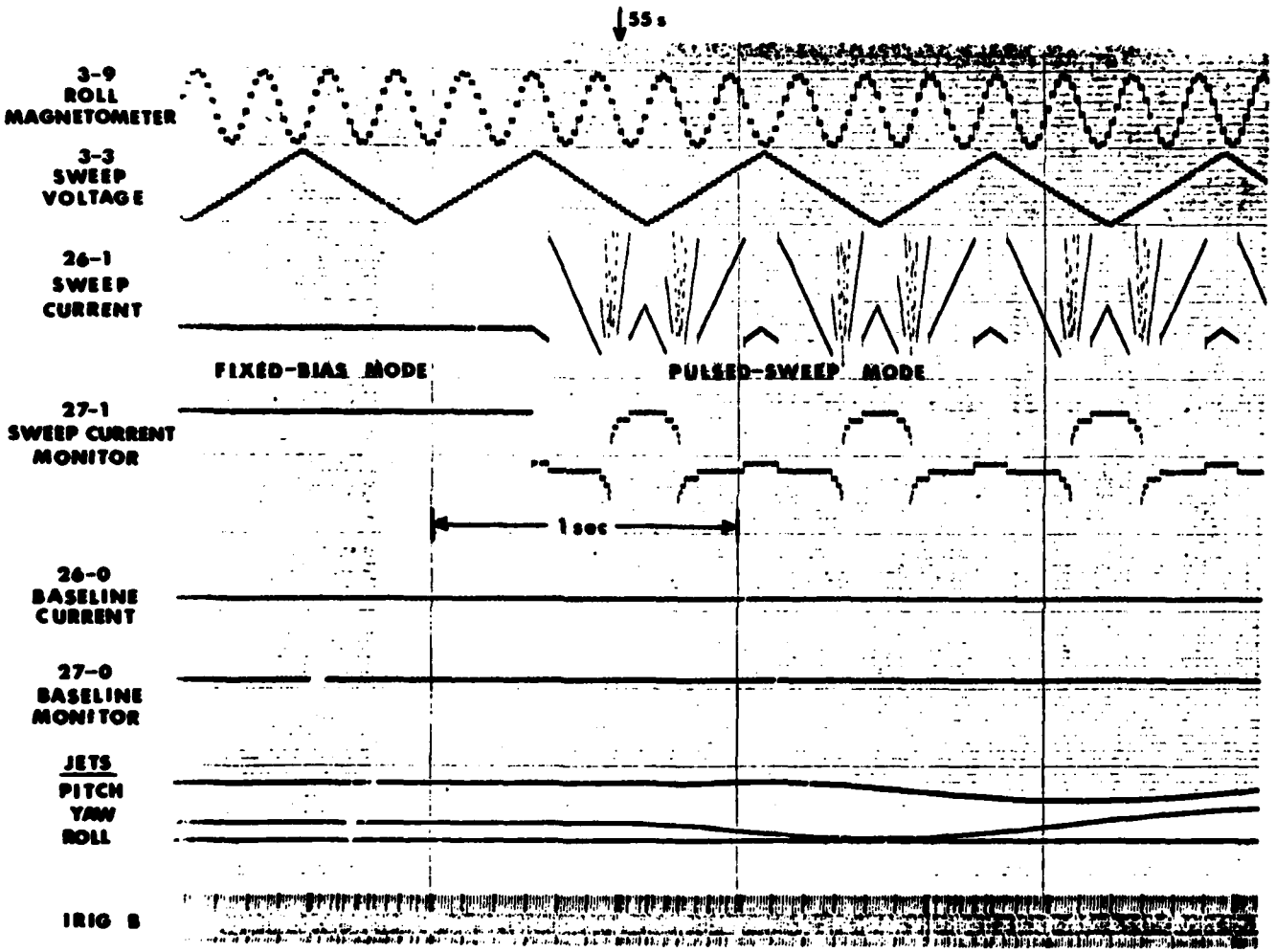

Fig. 4 — Analog record of PLUMEX I telemetry channels (3-9, 3-3, etc.) illustrating pulsed-plasma-probe outputs and relevant vehicle information (roll-magnetometer, attitude control jets and IRIG B timing). The probe electrometers (26-1) cover six decades of current in 8 automatic-switching ranges (26-1 shows automatic ranging, while 27-1 identifies each range through a simple algorithm). 9 bit accuracy is maintained throughout.

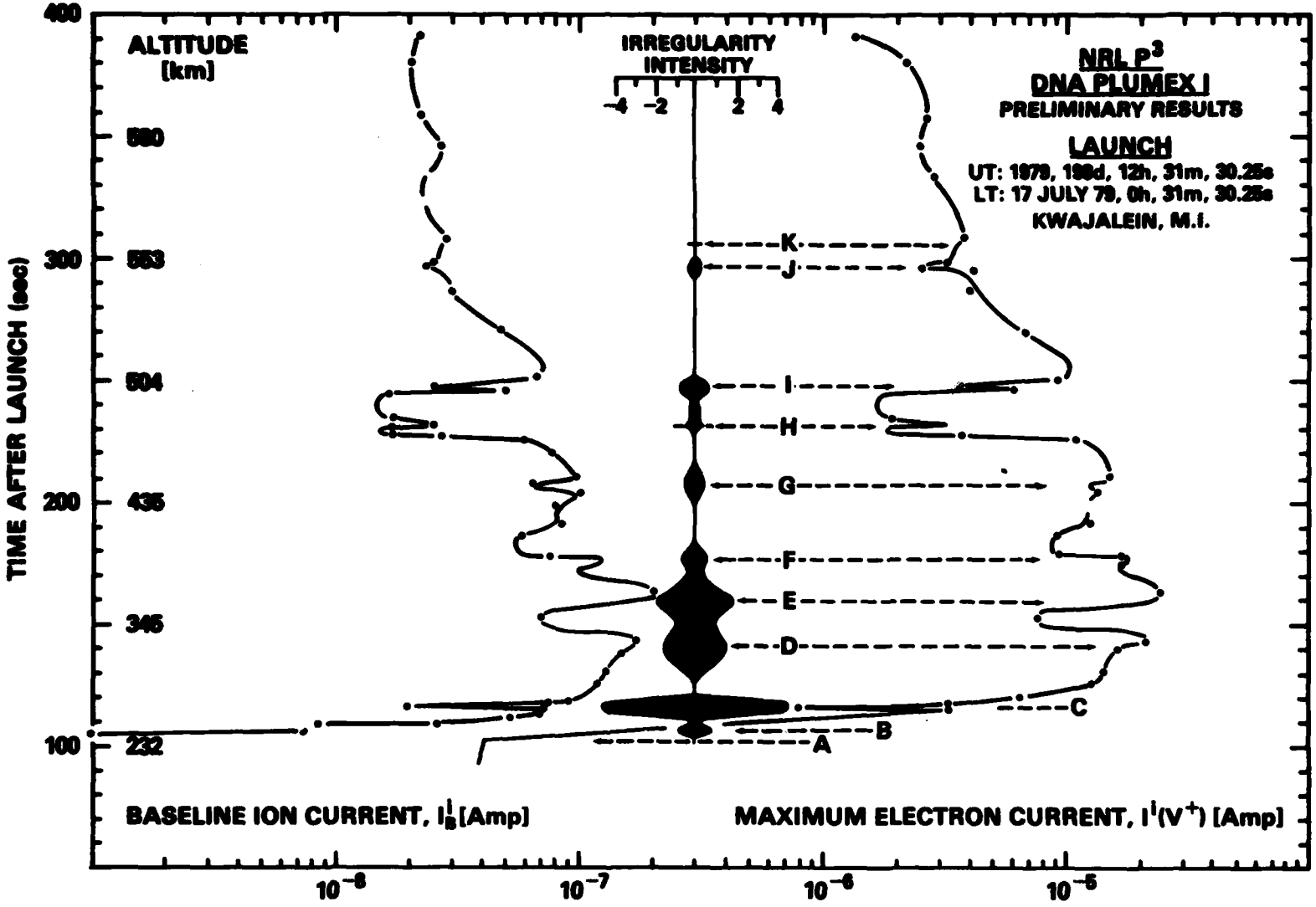

Fig. 5 — Relative electron density profile of macroscale features as measured simultaneously by ion and electron saturation probe currents collected on the upleg trajectory of PLUMEX I. The "irregularity intensity" provides a measure of smaller scale structure with a ± 4 intensity approximately equal to ± 80% fluctuations about a linear detrend.

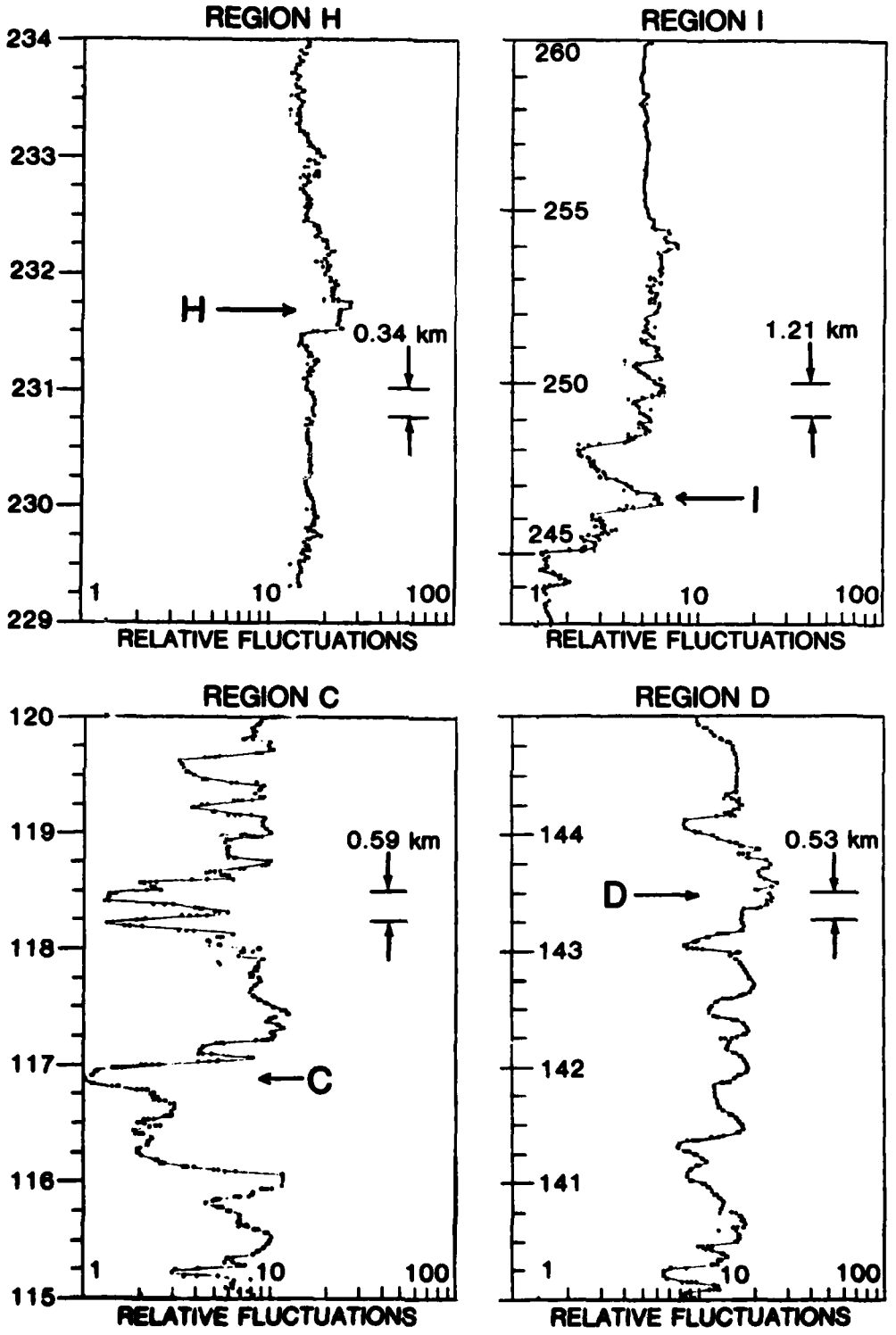

Fig. 6 — Expanded views of density fluctuations observed in regions C,D,H and I of Fig. 5

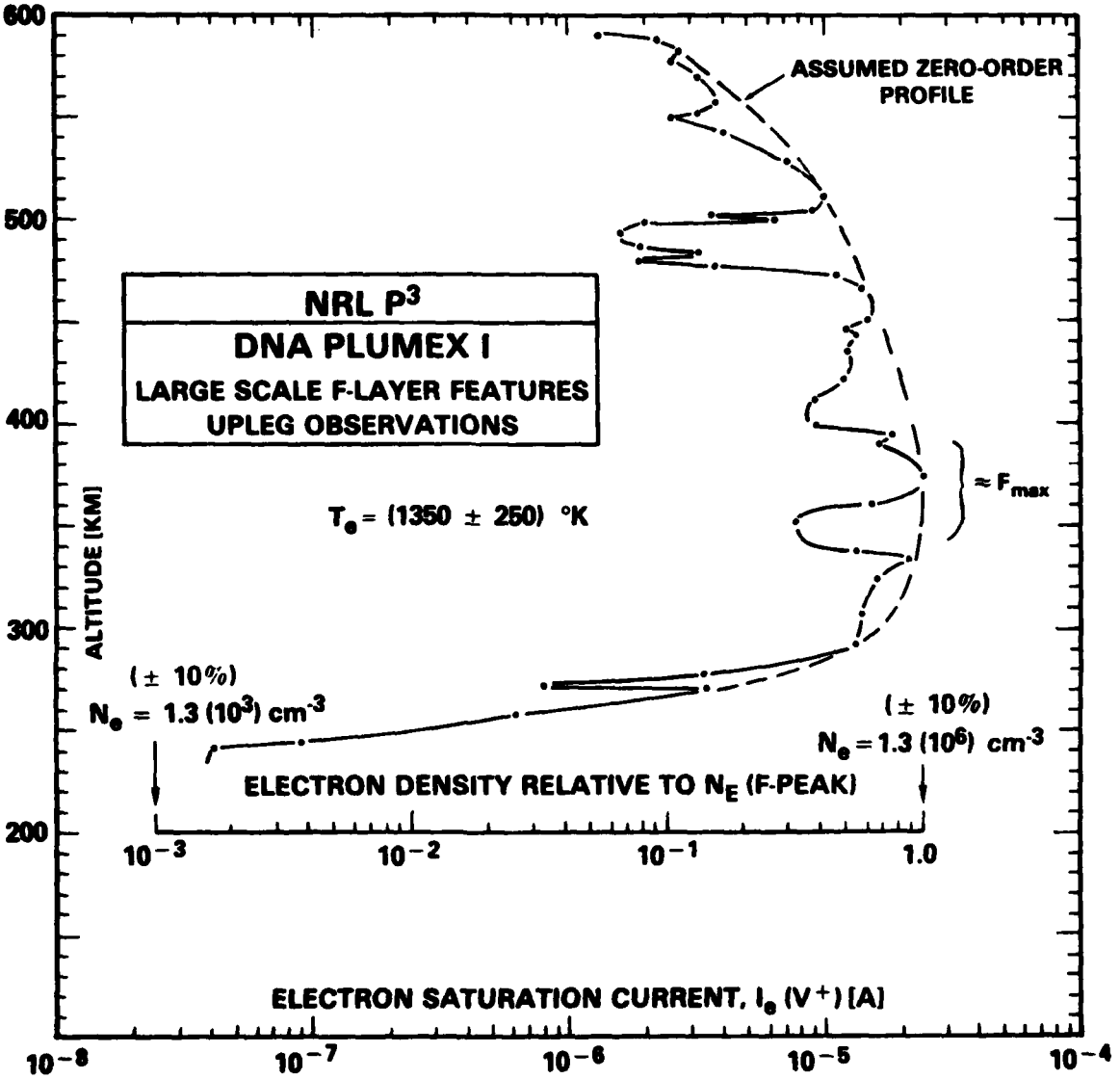

Fig. 7 — Relative and absolute profile of electron density (PLUMEX I upleg)

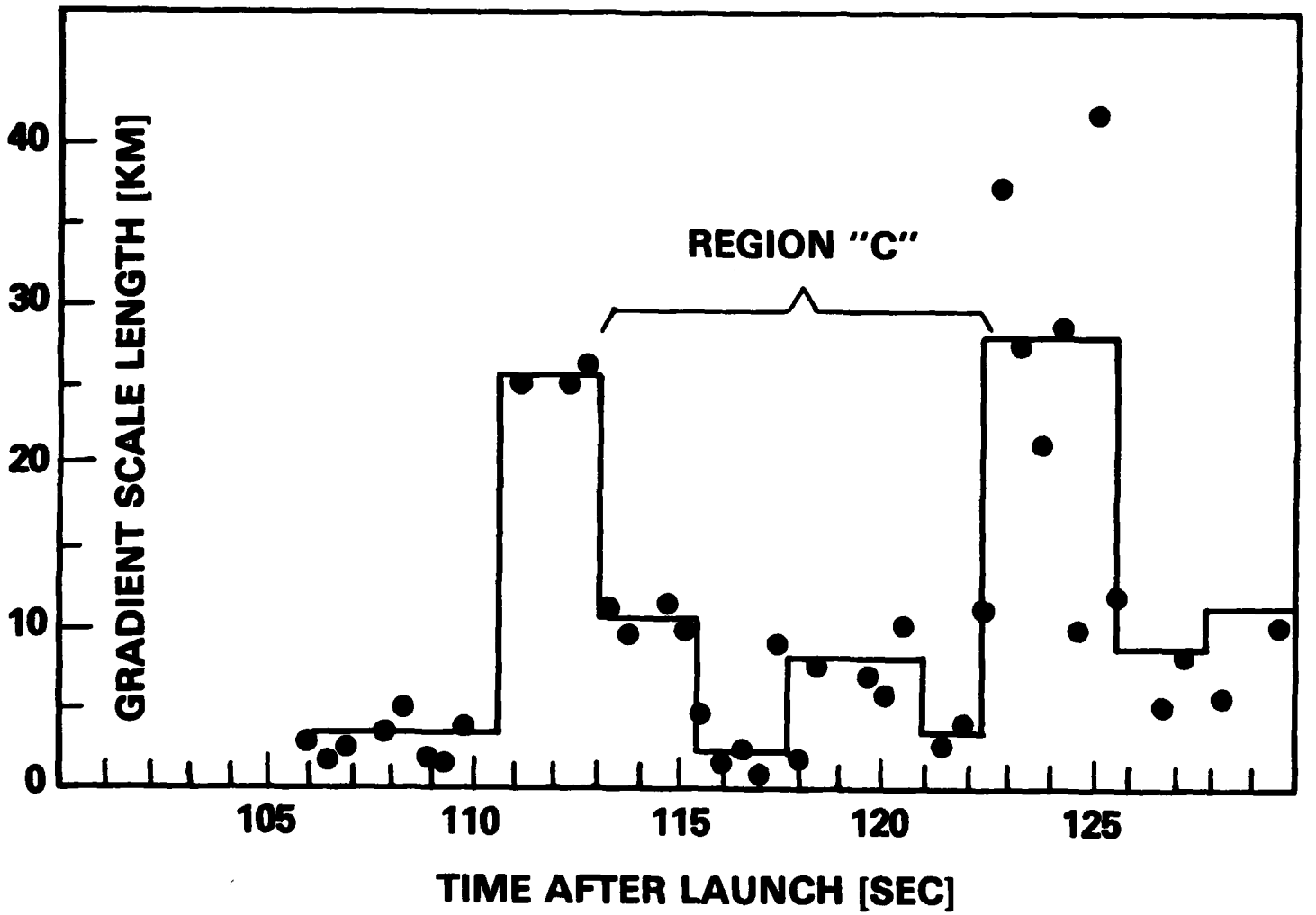

Fig. 8 — Gradient scale lengths $\left(L = \left[\frac{1}{N_e^o}\ \frac{dN_e^o}{dy}\right]^{-1}\right)$ on the bottomside gradient of the F-region layer shown in Figs. 5 and 6

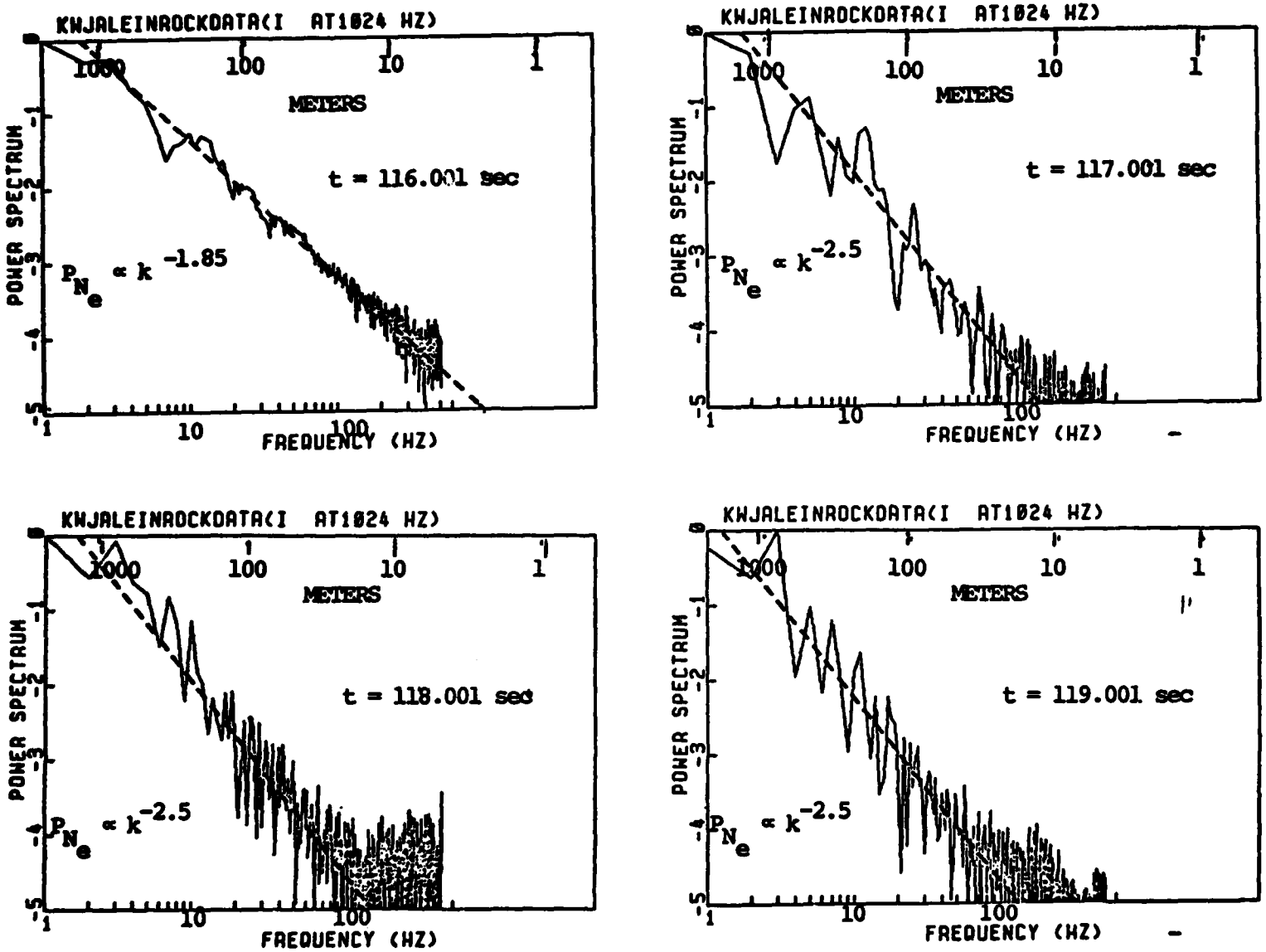

Fig. 9 — Power spectial analyses of density fluctuations in region "C" (Fig. 5)

DISTRIBUTION LIST

DEPARTMENT OF DEFENSE

ASSISTANT SECRETARY OF DEFENSE
COMM, DMD, CONT & INTELL
WASHINGTON, D.C. 20301
01CY ATTN J. BABCOCK
01CY ATTN M. EPSTEIN

ASSISTANT TO THE SECRETARY OF DEFENSE
ATOMIC ENERGY
WASHINGTON, D.C. 20301
01CY ATTN EXECUTIVE ASSISTANT

DIRECTOR
COMMAND CONTROL TECHNICAL CENTER
PENTAGON RM BE 685
WASHINGTON, D.C. 20301
01CY ATTN C-650
01CY ATTN C-312 R. MASON

DIRECTOR
DEFENSE ADVANCED RSCH PROJ AGENCY
ARCHITECT BUILDING
1400 WILSON BLVD.
ARLINGTON, VA. 22209
01CY ATTN NUCLEAR MONITORING RESEARCH
01CY ATTN STRATEGIC TECH OFFICE

DEFENSE COMMUNICATION ENGINEER CENTER
1860 WIEHLE AVENUE
RESTON, VA. 22290
01CY ATTN CODE R820
01CY ATTN CODE R410 JAMES W. MCLEAN
01CY ATTN CODE R720 J. WORTHINGTON

DEPT. OF THE AIR FORCE
HEADQUARTERS SPACE DIVISION
(AFSC) LOS ANGELES AIR FORCE STATION
P.O. BOX 92960
LOS ANGELES, CA 90009
01CY DIRECTOR, STP,
COL D.E. THURSBY
01CY MAJ C. JUND

DIRECTOR
DEFENSE INTELLIGENCE AGENCY
WASHINGTON, D.C. 20301
01CY ATTN DT-1B
01CY ATTN DB-4C E. O'FARRELL
01CY ATTN DIAAP A. WISE
01CY ATTN DIAST-5
01CY ATTN DT-1BZ R. MORTON
01CY ATTN HQ #-TR J. STEWART
01CY ATTN W. WITTIG DC-7D

DIRECTOR
DEFENSE NUCLEAR AGENCY
WASHINGTON, D.C. 20305
01CY ATTN STVL
04CY ATTN TITL
01CY ATTN DDST
03CY ATTN RAAE

COMMANDER
FIELD COMMAND
DEFENSE NUCLEAR AGENCY
KIRTLAND AFB, NM 87115
01CY ATTN FCPR

DIRECTOR
INTERSERVICE NUCLEAR WEAPONS SCHOOL
KIRTLAND AFB, NM 87115
01CY ATTN FCPR

DIRECTOR
JOINT STRAT TGT PLANNING STAFF
OFFUTT AFB
OMAHA, NB 68113
01CY ATTN JLTW-2
01CY ATTN JPST G. GOETZ

JOINT CHIEFS OF STAFF
WASHINGTON, D.C. 20301
01CY ATTN J-3 WWMCCS EVALUATION
OFFICE

CHIEF
LIVERMORE DIVISION FLD COMMAND DNA
DEPARTMENT OF DEFENSE
LAWRENCE LIVERMORE LABORATORY
P.O. BOX 808
LIVERMORE, CA 94550
01CY ATTN FCPRL

DIRECTOR
NATIONAL SECURITY AGENCY
DEPARTMENT OF DEFENSE
FT. GEORGE G. MEADE, MD 20755
01CY ATTN JOHN SKILLMAN R52
01CY ATTN FRANK LEONARD
01CY ATTN W14 PAT CLARK
01CY ATTN OLIVER H. BARTLETT W32
01CY ATTN R5

COMMANDANT
NATO SCHOOL (SHAPE)
APO NEW YORK 09172
01CY ATTN U.S. DOCUMENTS OFFICER

68-Blank

COMMANDER
U.S. ARMY COMM-ELEC ENGRG INSTAL AGY
FT. HUACHUCA, AZ 85613
01CY ATTN CCC-EMEO GEORGE LANE

COMMANDER
U.S. ARMY FOREIGN SCIENCE & TECH CTR
220 7TH STREET, NE
CHARLOTTESVILLE, VA 22901
01CY ATTN DRXST-SD
01CY ATTN R. JONES

COMMANDER
U.S. ARMY MATERIAL DEV & READINESS CMD
5001 EISENHOWER AVENUE
ALEXANDRIA, VA 22333
01CY ATTN DRCLDC J.A. BENDER

COMMANDER
U.S. ARMY NUCLEAR AND CHEMICAL AGENCY
7500 BACKLICK ROAD
BLDG. 2073
SPRINGFIELD, VA 22150
01CY ATTN LIBRARY

DIRECTOR
U.S. ARMY BALLISTIC RESEARCH LABS
ABERDEEN PROVING GROUND, MD 21005
01CY ATTN TECH LIB EDWARD BAICY

COMMANDER
U.S. ARMY SATCOM AGENCY
FT. MONMOUTH, NJ 07703
01CY ATTN DOCUMENT CONTROL

COMMANDER
U.S. ARMY MISSILE INTELLIGENCE AGENCY
REDSTONE ARSENAL, AL 35809
01CY ATTN JIM GAMBLE

DIRECTOR
U.S. ARMY TRADOC SYSTEMS ANALYSIS ACTIVITY
WHITE SANDS MISSILE RANGE, NM 88002
01CY ATTN ATAA-SA
01CY ATTN TCC/F. PAYAN JR.
01CY ATTN ATAA-TAC LTC. J. HESSE

COMMANDER
NAVAL ELECTRONIC SYSTEMS COMMAND
WASHINGTON, D.C. 20360
01CY ATTN NAVLEX 034 T. HUGHES
01CY ATTN PME 117
01CY ATTN PME 117-T
01CY ATTN CODE 5011
01CY ATTN PME-106-T

UNDER SECY OF DEF FOR RSCH & ENGR.
DEPARTMENT OF DEFENSE
WASHINGTON, D.C. 20301
01CY ATTN STRATEGIC & SPACE SYSTEMS (OS)

WWMCCS SYSTEM ENGINEERING ORG.
WASHINGTON, D.C. 20305
01CY ATTN R. CRAWFORD

COMMANDER/DIRECTOR
ATMOSPHERIC SCIENCES LABORATORY
U.S. ARMY ELECTRONICS COMMAND
WHITE SANDS MISSILE RANGE, NM 88002
01CY ATTN DELAS-EO F. NILES

DIRECTOR
BMD ADVANCED TECH CTR
HUNTSVILLE OFFICE
P.O. BOX 1500
HUNTSVILLE, AL 35807
01CY ATTN ATC-T MELVIN T. CAPPS
01CY ATTN ATC-O W. DAVIES
01CY ATTN ATC-R DON RUSS

PROGRAM MANAGER
BMD PROGRAM OFFICE
5001 EISENHOWER AVENUE
ALEXANDRIA, VA 22333
01CY ATTN DACS-BMT J. SHEA

CHIEF C-E SERVICE DIVISION
U.S. ARMY COMMUNICATIONS CMD
PENTAGON RM. 1B269
WASHINGTON, D.C. 20310
01CY ATTN C-E-SERVICES DIVISION

COMMANDER
FRADCOM TECHNICAL SUPPORT ACTIVITY
DEPARTMENT OF THE ARMY
FORT MONMOUTH, N.J. 07703
01CY ATTN DRSEL-NL-RD H. BENNET
01CY ATTN DRSEL-PL-ENV H. BOMKE
01CY ATTN J.E. QUIGELY

COMMANDER
HARRY DIAMOND LABORATORIES
DEPARTMENT OF THE ARMY
2800 POWDER MILL ROAD
ADELPHI, MD 20783
(CNWDI-INNER ENVELOPE: ATTN: DELHD-RBH)
01CY ATTN DELHD-TI M. WEINER
01CY ATTN DELHD-RB R. WILLIAMS
01CY ATTN DELHD-NP F. WIMENITZ
01CY ATTN DELHD-NP C. MOAZED

COMMANDING OFFICER
NAVAL INTELLIGENCE SUPPORT CTR
4301 SUITLAND ROAD, BLDG. 5
WASHINGTON, D.C. 20390
01CY ATTN MR. DUBBIN STIC 12
01CY ATTN NISC-50
01CY ATTN CODE 5404 J. GALET

COMMANDER
NAVAL SURFACE WEAPONS CENTER
DAHLGREN LABORATORY
DAHLGREN, VA 22448
01CY ATTN CODE DF-14 R. BUTLER

COMMANDING OFFICER
NAVY SPACE SYSTEMS ACTIVITY
P.O. BOX 92960
WORLDWAY POSTAL CENTER
LOS ANGLES, CA 90009
01CY ATTN CODE 52

OFFICE OF NAVAL RESEARCH
ARLINGTON, VA 22217
01CY ATTN CODE 465
01CY ATTN CODE 461
01CY ATTN CODE 402
01CY ATTN CODE 420
01CY ATTN CODE 421

COMMANDER
AEROSPACE DEFENSE COMMAND/DC
DEPARTMENT OF THE AIR FORCE
ENT AFB, CO 80912
01CY ATTN DC MR. LONG

COMMANDER
AEROSPACE DEFENSE COMMAND/XPD
DEPARTMENT OF THE AIR FORCE
ENT AFB, CO 80912
01CY ATTN XPDQQ
01CY ATTN XP

AIR FORCE GEOPHYSICS LABORATORY
HANSCOM AFB, MA 01731
01CY ATTN OPR HAROLD GARDNER
01CY ATTN OPR-1 JAMES C. ULWICK
01CY ATTN LKB KENNETH S. W. CAMPION
01CY ATTN OPR ALVA T. STAIR
01CY ATTN PHD JURGEN BUCHAU
01CY ATTN PHD JOHN P. MULLEN

AF WEAPONS LABORATORY
KIRTLAND AFB, NM 87117
01CY ATTN SUL
01CY ATTN CA AUTHER H. GUENTHER
01CY ATTN DYC CAPT. J. BARRY
01CY ATTN DYC JOHN M. KAMM
01CY ATTN DYT CAPT MARK A. FRY
01CY ATTN DES MAJ GARY GAHONG
01CY ATTN DYC J. JANNI

AFTAX
PATRICK AFB, FL 32925
01CY ATTN TF/MAJ WILEY
01CY ATTN TN

AIR FORCE WRIGHT AERONAUTICAL LABORATORIES
WRIGHT-PATTERSON AFB, OH 45433
01CY ATTN AAAD, WADE HUNT
01CY ATTN AAAD, ALLEN JOHNSON

DEPUTY CHIEF OF STAFF
RESEARCH, DEVELOPMENT, & ACQ
DEPARTMENT OF THE AIR FORCE
WASHINGTON, D.C. 20330
01CY ATTN AFRDQ

HEADQUARTERS
ELECTRONIC SYSTEMS DIVISION/XR
DEPARTMENT OF THE AIR FORCE
HANSCOM AFG, MA 01731
01CY ATTN XR J. DEAS

HEADQUARTERS
ELECTRONIC SYSTEMS DIVISION/YSEA
DEPARTMENT OF THE AIR FORCE
HANSCOM AFB, MA 01731
01CY ATTN YSEA

COMMANDER
NAVAL OCEAN SYSTEMS CENTER
SAN DIEGO, CA 92152
03CY ATTN CODE 532 W. MOLER
01CY ATTN CODE 0230 C. BAGGETT
01CY ATTN CODE 81 R. EASTMAN
01CY ATTN CODE 2200 M. RICHTER

DIRECTOR
NAVAL RESEARCH LABORATORY
WASHINGTON, D.C. 20375
01CY CODE 4100
01CY CODE 4101
01CY CODE 4120
01CY CODE 4701 JACK D. BROWN
20CY CODE 2626

01CY CODE 4732 E. MCLEAN
01CY CODE 6000
01CY CODE 7000
01CY CODE 7500
01CY CODE 7580
01CY CODE 7551
01CY CODE 7555
01CY CODE 7900

COMMANDER
NAVAL SEA SYSTEMS COMMAND
WASHINGTON, D.C. 20362
01CY ATTN CAPT. R. PITKIN

COMMANDER
NAVAL SPACE SURVEILLANCE SYSTEM
DAHLGREN, VA 22448
01CY ATTN CAPT. J.H. BURTON

OFFICER-IN-CHARGE
NAL SURFACE WEAPONS CENTER
WHITE OAK, SILVER SPRING, MD 20910
01CY ATTN CODE F31

DIRECTOR STRATEGIC SYSTEMS PROJECT OFFICE
DEPARTMENT OF THE NAVY
WASHINGTON, D.C. 20376
01CY ATTN NSP-2141
01CY ATTN NSSP-2722 FRED WIMBERLY

NAVAL SPACE SYSTEM ACTIVITY
P.O. BOX 92960
WORLDWAY POSTAL CENTER
LOS ANGELES, CA 90009
01CY ATTN LCDR DONALD SMODDY
01CY ATTN COMMANDING OFFICER

HEADQUARTERS
ELECTRONIC SYSTEMS DIVISION/DC
DEPARTMENT OF THE AIR FORCE
HANSCOM AFB, MA 01731
01CY ATTN DCKC MAJ J.C. CLARK

COMMANDER
FOREIGN TECHNOLOGY DIVISION, AFSC
WRIGHT-PATTERSON AFB, OH 45433
01CY ATTN NICD LIBRARY
01CY ATTN ETDP B. BALLARD

COMMANDER
ROME AIR DEVELOPMENT CENTER, AFSC
GRIFFISS AFB, NY 13441
01CY ATTN DOC LIBRARY/TSLD
01CY ATTN OCSE V. COYNE

SAMSO/SZ
POST OFFICE BOX 92960
WORLDWAY POSTAL CENTER
LOS ANGELES, CA 90009
(SPACE DEFENSE SYSTEMS)
01CY ATTN SZJ

STRATEGIC AIR COMMAND/XPFS
OFFUTT AFB, NB 68113
01CY ATTN XPFS MAJ B. STEPHAN
01CY ATTN ADWATE MAJ. BRUCE BAUER
01CY ATTN NRT
01CY ATTN DOK CHIEF SCIENTIST

SAMSO/YA
P.O. BOX 92960
WORLDWAY POSTAL CENTER
LOS ANGELES, CA 90009
01CY ATTN YAT CAPT L. BLACKWELDER

SAMSO/SK
P.O. BOX 92960
WORLDWAY POSTAL CENTER
LOS ANGELES, CA 90009
01CY ATTN SKA (SPACE COMM SYSTEMS) M. CLAVIN

SAMSO/MN
NORTON AFB, CA 92409
(MINUTEMAN)
01CY ATTN MNNL LTC KENNEDY

COMMANDER
ROME AIR DEVELOPMENT CENTER, AFSC
HANSCOM AFB, MA 01731
01CY ATTN EEP A. LORENTZEN

DEPARTMENT OF ENERGY

DEPARTMENT OF ENERGY
ALBUQUERQUE OPERATIONS OFFICE
P.O. BOX 5400
ALBUQUERQUE, NM 87115
01CY ATTN DOC CON FOR D. SHERWOOD

DEPARTMENT OF ENERGY
LIBRARY ROOM G-042
WASHINGTON, D.C. 20545
01CY ATTN DOC CON FOR A. LABOWITZ

EG&G, INC.
LOS ALAMOS DIVISION
P.O. BOX 809
LOS ALAMOS, NM 85544
01CY ATTN DOC CON FOR J. BREEDLOVE

UNIVERSITY OF CALIFORNIA
LAWRENCE LIVERMORE LABORATORY
P.O. BOX 808
LIVERMORE, CA 94550
01CY ATTN DOC CON FOR TECH INFO DEPT
01CY ATTN DOC CON FOR L-389 R. OTT
01CY ATTN DOC CON FOR L-31 R. HAGER
01CY ATTN DOC CON FOR L-46 F. SEWARD

LOS ALAMOS SCIENTIFIC LABORATORY
P.O. BOX 1663
LOS ALAMOS, NM 87545
01CY ATTN DOC CON FOR J. WOLCOTT
01CY ATTN DOC CON FOR R.F. TASCHEK
01CY ATTN DOC CON FOR E. JONES
01CY ATTN DOC CON FOR J. MALIK
01CY ATTN DOC CON FOR R. JEFFRIES
01CY ATTN DOC CON FOR J. ZINN
01CY ATTN DOC CON FOR P. KEATON
01CY ATTN DOC CON FOR D. WESTERVELT
01CY ATTN DOC CON FOR M. PONGRATZ

SANDIA LABORATORIES
P.O. BOX 5800
ALBUQUERQUE, NM 87115
01CY ATTN DOC CON FOR J. MARTIN
01CY ATTN DOC CON FOR W. BROWN
01CY ATTN DOC CON FOR A. THORNBROUGH
01CY ATTN DOC CON FOR T. WRIGHT
01CY ATTN DOC CON FOR D. DAHLGREN
01CY ATTN DOC CON FOR 3141
01CY ATTN DOC CON FOR SPACE PROJECT DIV

SANDIA LABORATORIES
LIVERMORE LABORATORY
P.O. BOX 969
LIVERMORE, CA 94550
01CY ATTN DOC CON FOR B. MURPHY
01CY ATTN DOC CON FOR T. COOK

OFFICE OF MILITARY APPLICATION
DEPARTMENT OF ENERGY
WASHINGTON, D.C. 20545
01CY ATTN DOC CON FOR D. GALE

OTHER GOVERNMENT

CENTRAL INTELLIGENCE AGENCY
ATTN RD/SI, RM 5G48, HQ BLDG
WASHINGTON, D.C. 20505
01CY ATTN OSI/PSID RM 5F 19

DEPARTMENT OF COMMERCE
NATIONAL BUREAU OF STANDARDS
WASHINGTON, D.C. 20234
(ALL CORRES: ATTN SEC OFFICER FOR)
01CY ATTN R. MOORE

DEPARTMENT OF TRANSPORTATION
OFFICE OF THE SECRETARY
TAD-44.1, ROOM 10402-B
400 7TH STREET, S.W.
WASHINGTON, D.C. 20590
01CY ATTN R. LEWIS
01CY ATTN R. DOHERTY

INSTITUTE FOR TELECOM SCIENCES
NATIONAL TELECOMMUNICATIONS & INFO ADMIN
BOULDER, CO 80303
01CY ATTN A. JEAN (UNCLASS ONLY)
01CY ATTN W. UTLAUT
01CY ATTN D. CROMBIE
01CY ATTN L. BERRY

NATIONAL OCEANIC & ATMOSPHERIC ADMIN
ENVIRONMENTAL RESEARCH LABORATORIES
DEPARTMENT OF COMMERCE
BOULDER, CO 80302
01CY ATTN R. GRUBB
01CY ATTN AERONOMY LAB G. REID

DEPARTMENT OF DEFENSE CONTRACTORS

AEROSPACE CORPORATION
P.O. BOX 92957
LOS ANGELES, CA 90009
01CY ATTN I. GARFUNKEL
01CY ATTN T. SALMI
01CY ATTN V. JOSEPHSON
01CY ATTN S. BOWER
01CY ATTN N. STOCKWELL
01CY ATTN D. OLSEN
01CY ATTN J. CARTER
01CY ATTN F. MORSE
01CY ATTN SMFA FOR PWW
01CY ATTN J. FENNEL
01CY ATTN C. RICE
01CY ATTN H. KOONS

ANALYTICAL SYSTEMS ENGINEERING CORP
5 OLD CONCORD ROAD
BURLINGTON, MA 01803
01CY ATTN RADIO SCIENCES

BERKELEY RESEARCH ASSOCIATES, INC.
P.O. BOX 983
BERKELEY, CA 94701
01CY ATTN J. WORKMAN

BOEING COMPANY, THE
P.O. BOX 3707
SEATTLE, WA 98124
01CY ATTN G. KEISTER
01CY ATTN D. MURRAY
01CY ATTN G. HALL
01CY ATTN J. KENNEY

CALIFORNIA AT SAN DIEGO, UNIV OF
IPAPS, B-019
LA JOLLA, CA 92093
01CY ATTN HENRY G. BOOKER
01CY ATTN E.C. WHIPPLE

BROWN ENGINEERING COMPANY, INC.
CUMMINGS RESEARCH PARK
HUNTSVILLE, AL 35807
01CY ATTN ROMEO A. DELIBERIS

CHARLES STARK DRAPER LABORATORY, INC.
555 TECHNOLOGY SQUARE
CAMBRIDGE, MA 02139
01CY ATTN D.B. COX
01CY ATTN J.P. GILMORE

COMPUTER SCIENCES CORPORATION
6565 ARLINGTON BLVD
FALLS CHURCH, VA 22046
01CY ATTN H. BLANK
01CY ATTN JOHN SPOOR
01CY ATTN C. NAIL

COMSAT LABORATORIES
LINTHICUM ROAD
CLARKSBURG, MD 20734
01CY ATTN G. HYDE

ELECTROSPACE SYSTEMS, INC.
BOX 1359
RICHARDSON, TX 75080
01CY ATTN H. LOGSTON
01CY ATTN SECURITY (PAUL PHILLIPS)

ESL INCL.
495 JAVA DRIVE
SUNNYVALE, CA 94086
01CY ATTN J. ROBERTS
01CY ATTN JAMES MARSHALL
01CY ATTN C.W. PRETTIE

FORD AEROSPACE AND COMMUNICATIONS CORP
3939 FABIAN WAY
PALO ALOT, CA 94303
01CY ATTN J.T. MATTINGLEY

GENERAL ELECTRIC COMPANY
SPACE DIVISION
VALLEY FORGE SPACE CENTER
GODDARD BLVD KING OF PRUSSIA
P.O. BOX 8555
PHILADELPHIA, PA 19101
01CY ATTN M.H. BORTNER SPACE SCI LAB

GENERAL ELECTRIC COMPANY
P.O. BOX 1122
SYRACUSE, NY 13201
01CY ATTN F. REIBERT

GENERAL ELECTRIC COMPANY
TEMPO-CENTER FOR ADVANCED STUDIES
816 STATE STREET (P.O. DRAWER QQ)
SANTA BARBARA, CA 93102
01CY ATTN DASIAC
01CY ATTN DON CHANDLER
01CY ATTN TOM BARRETT
01CY ATTN TIM STEPHANS
01CY ATTN WARREN S. KNAPP
01CY ATTN WILLIAM MCNAMARA
01CY ATTN B. GAMBILL
01CY ATTN MACK STANTON

GENERAL ELECTRIC TECH SERVICES CO., INC.
HMES
COURT
SYRACUSE, NY 13201
01CY ATTN G. MILLMAN

GENERAL RESEARCH CORPORATION
SANTA BARBARA DIVISION
P.O. BOX 6770
SANTA BARBARA, CA 93111
01CY ATTN JOE ISE JR
01CY ATTN JOEL GARBARINO

GEOPHYSICAL INSTITUTE
UNIVERSITY OF ALASKA
FAIRBANKS, AK 99701
(ALL CLASS ATTN: SECURITY OFFICERS)
01CY ATTN T.N. DAVIS (UNCL ONLY)
01CY ATTN NEAL BROWN (UNCL ONLY)
01CY ATTN TECHNICAL LIBRARY
01CY ATTN T. HALLINAN

GTE SYLVANIA, INC.
ELECTRONICS SYSTEMS GRP-EASTERN DIV
77 - STREET
NEEDHAM, MA 02194
01CY ATTN MARSHAL CROSS

ILLINOIS, UNIVERSITY OF
DEPARTMENT OF ELECTRICAL ENGINEERING
URBANA, IL 61803
01CY ATTN K. YEH

INSTITUTE FOR DEFENSE ANALYSES
400 ARMY-NAVY DRIVE
ARLINGTON, VA 22202
01CY ATTN J.M. AEIN
01CY ATTN HANS WOLFHARD
01CY ATTN JOEL BENGSTON

HSS, INC.
2 ALFRED CIRCLE
BEDFORD, MA 01730
01CY ATTN DONALD HANSEN

INTL TEL & TELEGRAPH CORPORATION
500 WASHINGTON AVENUE
NUTLEY, NJ 07110
01CY ATTN TECHNICAL LIBRARY

JAYCOR
1401 CAMINO DEL MAR
DEL MAR, CA 92014
01CY ATTN S.R. GOLDMAN

JOHNS HOPKINS UNIVERSITY
APPLIED PHYSICS LABORATORY
JOHNS HOPKINS ROAD
LAUREL, MD 20810
01CY ATTN DOCUMENT LIBRARIAN
01CY ATTN THOMAS POTEMRA
01CY ATTN JOHN DASSOULAS

LOCKHEED MISSILES & SPACE CO INC
P.O. BOX 504
SUNNYVALE, CA 94088
01CY ATTN DEPT 60-12
01CY ATTN D.R. CHURCHILL

LOCKHEED MISSILES AND SPACE CO INC
3251 HANOVER STREET
PALO ALTO, CA 94304
01CY ATTN MARTIN WALT DEPT 52-10
01CY ATTN RICHARD G. JOHNSON DEPT 52-12
01CY ATTN W.L. IMHOF DEPT 52-12
01CY ATTN D. CAUFMAN

KAMAN SCIENCES CORP
P.O. BOX 7463
COLORADO SPRINGS, CO 80933
01CY ATTN T. MEAGHER

LINKABIT CORP
10453 ROSELLE
SAN DIEGO, CA 92121
01CY ATTN IRWIN JACOBS
01CY ATTN I. ROTHMUELLER

LOWELL RSCH FOUNDATION, UNIVERSITY OF
450 AIKEN STREET
LOWELL, MA 01854
01CY ATTN K. BIBL
01CY ATTN B. REINISCH

M.I.T. LINCOLN LABORATORY
P.O. BOX 73
LEXINGTON, MA 02173
01CY ATTN DAVID M. TOWLE
01CY ATTN P. WALDRON
01CY ATTN L. LOUGHLIN
01CY ATTN D. CLARK
01CY ATTN J. DAVIS

MARTIN MARIETTA CORP
ORLANDO DIVISION
P.O. BOX 5837
ORLANDO, FL 32805
01CY ATTN R. HEFFNER

MCDONNELL DOUGLAS CORPORATION
5301 BOLSA AVENUE
HUNTINGTON BEACH, CA 92647
01CY ATTN N. HARRIS
01CY ATTN J. MOULE
01CY ATTN GEORGE MROZ
01CY ATTN W. OLSON
01CY ATTN R.W. HALPRIN
01CY ATTN TECHNICAL LIBRARY SERVICES

MISSION RESEARCH CORPORATION
735 STATE STREET
SANTA BARBARA, CA 93101
01CY ATTN P. FISCHER
01CY ATTN W.F. CREVIER
01CY ATTN STEVEN L. GUTSCHE
01CY ATTN D. SAPPENFIELD
01CY ATTN R. BOGUSCH
01CY ATTN RALPH KILB
01CY ATTN R. HENDRICK
01CY ATTN DAVE SOWLE
01CY ATTN F. FAJEN
01CY ATTN M. SCHEIBE
01CY ATTN CONRAD L. LONGMIRE
01CY ATTN WARREN A. SCHLUETER

MITRE CORPORATION, THE
P.O. BOX 208
BEDFORD, MA 01730
01CY ATTN JOHN MORGANSTERN
01CY ATTN G. HARDING
01CY ATTN C.E. CALLAHAN

MITRE CORP
WESTGATE RESEARCH PARK
1820 DOLLY MADISON BLVD
MCLEAN, VA 22101
01CY ATTN W. HALL
01CY ATTN W. FOSTER

PACIFIC-SIERRA RESEARCH CORP
1456 CLOVERFIELD BLVD.
SANTA MONICA, CA 90404
01CY ATTN E.C. FIELD JR

PENNSYLVANIA STATE UNIVERSITY
IONISPHERE RESEARCH LAB
318 ELECTRICAL ENGINEERING EAST
UNIVERSITY PARK, PA 16802
(NO CLASSIFIED TO THIS ADDRESS)
01CY ATTN IONOSPHERIC RESEARCH LAB

PHOTOMETRICS, INC.
442 MARRETT ROAD
LEXINGTON, MA 02173
01CY ATTN IRVING L. KOFSKY

PHYSICAL DYNAMICS INC.
P.O. BOX 3027
BELLEVUE, WA 98009
01CY ATTN E.J. FREMOUW

PHYSICAL DYNAMICS INC.
P.O. BOX 1069
BERKELEY, CA 94701
01CY ATTN A. THOMPSON

R & D ASSOCIATES
P.O. BOX 9695
MARINA DEL REY, CA 90291
01CY ATTN FORREST GILMORE
01CY ATTN BRYAN GABBARD
01CY ATTN WILLIAM B. WRIGHT JR.
01CY ATTN WILLIAM J. KARZAS
01CY ATTN ROBERT F. LELEVIER
01CY ATTN H. ORY
01CY ATTN C. MACDONALD
01CY ATTN R. TURCO

RAND CORPORATION, THE
1700 MAIN STREET
SANTA MONICA, CA 90406
01CY ATTN CULLEN CRAIN
01CY ATTN ED BEDROZIAN

RIVERSIDE RESEARCH INSTITUTE
80 WEST END AVENUE
NEW YORK, NY 10023
01CY ATTN VINCE TRAPANI

SCIENCE APPLICATION, INC.
P.O. BOX 2351
LAJOLLA, CA 92038
01CY ATTN LEWIS M. LINSON
01CY ATTN DANIEL A. HAMLIN
01CY ATTN D. SACHS
01CY ATTN E.A. STRAKER
01CY ATTN CURTUS A. SMITH
01CY ATTN JACK MCDOUGALL

RAYTHEON CO.
528 BOSTON POST ROAD
SUDBURY, MA 01776
01CY ATTN BARBARA ADAMS

SCIENCE APPLICATIONS, INC.
HUNTSVILLE DIVISION
2109 W. CLINTON AVENUE
SUITE 700
HUNTSVILLE, AL 35805
01CY ATTN DALE H. DAVIS

SCIENCE APPLICATIONS, INCORPORATED
8400 WESTPARK DRIVE
MCLEAN, VA 22101
01CY ATTN J. COCKAYNE

SCIENCE APPLICATIONS, INC.
80 MISSION DRIVE
PLEASANTON, CA 94566
01CY ATTN SZ

SRI INTERNATIONAL
333 RAVENSWOOD AVENUE
MENLO PARK, CA 94025
01CY ATTN DONARD NEILSON
01CY ATTN ALAN BURNS
01CY ATTN G. SMITH
01CY ATTN L.L. COBB
01CY DAVID A. JOHNSON
01CY ATTN WALTER G. CHESNUT
01CY ATTN CHARLES L. RINO
01CY ATTN WALTER JAYE
01CY ATTN N. BARON
01CY ATTN R. LIVINGSTON

01CY ATTN RAY L. LEADABRAND
01CY ATTN C. CARPENTER
01CY ATTN G. PRICE
01CY ATTN J. PETERSON
01CY ATTN R. HAKE, JR.
01CY ATTN V. GONZALES
01CY ATTN D. MCDANIEL
01CY ATTN R. TSUNODA

TECHNOLOGY INTERNATIONAL CORP
75 WIGGINS AVENUE
BEDFORD, MA 01730
01CY ATTN W.P. BOQUIST

UNIVERSITY OF TOKYO
ISAS
KOMABA, MEGURO-KU
TOKYO, JAPAN
01CY ATTN DR. K.I. OYAMA

MAX-PLANCK-INSTITUT
FUR PHYSIK UND ASTROPHYSIK
INSTITUT FUR EXTRATERRESTRICHE PHYSIK
8046 GARCHING B. MUNCHEN, GERMANY
01CY ATTN PROF. GERHARD HAERENDEL

TRW DEFENSE & SPACE SYS GROUP
ONE SPACE PARK
REDONDO BEACH, CA 90278
01CY ATTN R.K. PLEBUCH
01CY ATTN S. ALTSCHULER
01CY ATTN D. DEE

VISIDYNE, INC.
19 THIRD AVENUE
NORTH WEST INDUSTRIAL PARK
BURLINGTON, MA 01802
01CY ATTN CHARLES HUMPHREY
01CY ATTN J.W. CARPENTER

IONOSPHERIC MODELING DISTRIBUTION LIST
UNCLASSIFIED ONLY

PLEASE DISTRIBUTE ONE COPY (EXCEPT WHERE NOTED OTHERWISE) TO EACH OF THE FOLLOWING PEOPLE:

ADVANCED RESEARCH PROJECTS AGENCY (ARPA)
STRATEGIC TECHNOLOGY OFFICE
ARLINGTON, VA 22217

CAPT DONALD M. LEVINE

NAVAL RESEARCH LABORATORY
WASHINGTON, D.C. 20375

DR. R. MEIER - CODE 4141
DR. TIMOTHY COFFEY - CODE 4000
DR. S. OSSAKOW - CODE 4780
DR. J. GOODMAN - CODE 4180
DR. E. SZUSZCZEWICZ - CODE 4187 (50 COPIES)

DIRECTOR OF SPACE AND ENVIRONMENTAL LABORATORY
NOAA
BOULDER, CO 80302

DR. A. GLENN JEAN
DR. G. W. ADAMS
DR. D. N. ANDERSON
DR. K. DAVIES
DR. R. F. DONNELLY

AIR FORCE GEOPHYSICS LABORATORY
HANSCOM AIR FORCE BASE, MA 01731

DR. T. ELKINS
DR. W. SWIDER
MRS. R. SAGALYN
DR. J. M. FORBES
DR. T. J. KENESHEA
DR. J. AARONS
DR. R. NARCISI

OFFICE OF NAVAL RESEARCH
800 NORTH QUINCY STREET
ARLINGTON, VA 22217

U.S. ARMY ABERDEEN RESEARCH AND DEVELOPMENT
CENTER BALLISTIC RESEARCH LABORATORY
ABERDEEN, MD 21001

DR. J. HEIMERL

COMMANDER
NAVAL AIR SYSTEMS COMMAND
DEPARTMENT OF THE NAVY
WASHINGTON, D.C. 20360

DR. T. CZUBA

HARVARD UNIVERSITY
HARVARD SQUARE
CAMBRIDGE, MASS. 02138

DR. M. B. McELROY
DR. R. LINDZEN

PENNSYLVANIA STATE UNIVERSITY
UNIVERSITY PARK, PA 16802

DR. J. S. NISBET
DR. P. R. ROHRBAUGH
DR. D. E. BARAN
DR. L. A. CARPENTER
DR. M. LEE
DR. R. DIVANY
DR. P. BENNETT
DR. E. KLEVANS

UNIVERSITY OF CALIFORNIA, LOS ANGELES
405 HILLGARD AVENUE
LOS ANGELES, CA 90024

DR. R. STENZEL
DR. F. V. CORONITI
DR. C. KENNEL
DR. W. GEKELMAN

UNIVERSITY OF CALIFORNIA, BERKELEY
BERKELEY, CA 94720

DR. M. HUDSON

UTAH STATE UNIVERSITY
4TH AND 8TH STREETS
LOGAN, UTAH 84322

DR. P. M. BANKS
DR. R. HARRIS
DR. V. PETERSON
DR. R. MEGILL
DR. K. BAKER
DR. R. WILLIAMSON

CORNELL UNIVERSITY
ITHACA, N.Y. 14850

DR. W. E. SWARTZ
DR. R. SUDAN
DR. D. FARLEY
DR. M. KELLEY

NASA
GODDARD SPACE FLIGHT CENTER
GREENBELT, MD 20771

DR. S. J. BAUER/CODE 600
DR. R. HARTEL/CODE 621
DR. R. GOLDBERG/CODE 912
DR. S. CHANDRA
DR. K. MAEDO
DR. R. BENSON/CODE 621

PRINCETON UNIVERSITY
PLASMA PHYSICS LABORATORY
PRINCETON, N.J. 08540

DR. F. PERKINS
DR. E. FRIEMAN

INSTITUTE FOR DEFENSE ANALYSIS
400 ARMY/NAVY DRIVE
ARLINGTON, VA 22202

DR. E. BAUER

UNIVERSITY OF MARYLAND
COLLEGE PARK, MD 20742

DR. K. PAPADOPOULOS
DR. E. OTT

UNIVERSITY OF PITTSBURGH
PITTSBURGH, PA 15213

DR. N. ZABUSKY
DR. M. BIONDI

DEFENSE DOCUMENTATION CENTER
CAMERON STATION
ALEXANDRIA, VA 22314

(12 COPIES IF OPEN PUBLICATION
OTHERWISE 2 COPIES) 12 CY ATTN TC

UNIVERSITY OF CALIFORNIA
LOS ALAMOS SCIENTIFIC LABORATORY
J-10, MS-664
LOS ALAMOS, NEW MEXICO 87545

DR. M. PONGRATZ
DR. D. SIMONS
DR. G. BARASCH
DR. L. DUNCAN

OFFICE OF ASSISTANT SECRETARY OF NAVY
FOR RESEARCH, ENGINEERING AND SYSTEMS
PENTAGON RM 4D745
Washington, DC 20350

03 CY Attn Dr. H. Rabin
Deputy Assistant
Sec. of Navy